Greenhouse Gases: Science and Technology

ORIGINAL ARTICLE OPEN ACCESS

Carbon Storage in Fold-and-Thrust Belts: An Overlooked Gigatonne Storage Opportunity

Lars W. Koehn[1] | Ethan W. Conley[1] | Isabella Andrade[1] | Philip S. Prince[1] | Ryan M. Pollyea[1,2]

[1]Department of Geosciences, Virginia Polytechnic Institute & State University, Blacksburg, Virginia, USA | [2]Virginia Center for Coal and Energy Research, Virginia Polytechnic Institute & State University, Blacksburg, Virginia, USA

Correspondence: Lars W. Koehn (larsk@vt.edu)

Received: 13 January 2025 | **Revised:** 6 July 2025 | **Accepted:** 9 July 2025

Funding: This work was supported by the U.S. Department of Energy under Award Number DE-FE0031830 through the Southeast Regional Carbon Sequestration Partnership.

Keywords: Appalachian Basin | carbon storage | carbon capture and storage (CCS) | fold-and-thrust belts | Ouachita | Sub-Andes

ABSTRACT

This study presents numerical investigations of the trapping characteristics of fold-and-thrust belt structures, defining three carbon capture and storage (CCS) play types that could be used to store commercial volumes (millions of tonnes) of CO_2. Specifically, we present simulations of CO_2 storage in three fold-and-thrust belt models comprising a thrust-ramp, duplex, and thrust-fold geometry. To constrain these play types in realistic geology, each model is based on a study site, including a novel investigation of a greenfield saline reservoir in Virginia, USA, being considered for commercial carbon storage and two well-characterized petroleum fields: the Wilburton field in Oklahoma, USA, and the Incahuasi field in Bolivia. Our results provide insight into several key parameters, such as the long-term security of injected CO_2 in these geologies and injection strategies for maximizing storage efficiency while reducing pressure-related risk. These results improve the understanding of CCS in fold-and-thrust belt storage sites globally by describing general storage parameters that may be applied to site-specific projects. We find that thrust-ramp geometries may securely trap CO_2 through solubility and hydrodynamic trapping under suitable reservoir conditions, duplex structures may store some quantities of CO_2 but are pressure-constrained, and that thrust-ramp structures may store large quantities of CO_2 by maximizing fetch volume, which simultaneously lowers geomechanical risk by reducing pressure buildup along zones of weakness.

1 | Introduction

Carbon capture and storage (CCS) is the process of capturing CO_2 from the atmosphere or from point-sources and storing it in deep geologic formations. CCS is a key technology for heavy industry facilities, like cement and steel production which produce CO_2 as part of the manufacturing process and for reducing the emissions from fossil fuel-burning energy generation and chemical manufacturing [1]. Potential geologic formations include depleted petroleum reservoirs, deep saline aquifers, and mafic igneous formations [2]. Of these, sedimentary storage, that is, storage in depleted petroleum reservoirs or saline aquifers, has the greatest global distribution [3, 4] and highest potential storage volume [5]. Similar to petroleum resources, sedimentary carbon storage reservoirs require a geologic formation with sufficient porosity and permeability to facilitate the storage of large quantities of fluid, thousands to millions of tonnes of CO_2 per year, and a stratigraphic or structural barrier that prevents the fluid, for example, injected CO_2, from migrating to the surface [6]. Additionally, past CCS projects have injected CO_2 into formations that have sufficient pressure and temperature for CO_2 to be stored in a supercritical state, 31°C and 7.4 MPa, which keeps the CO_2 in

This is an open access article under the terms of the Creative Commons Attribution-NonCommercial-NoDerivs License, which permits use and distribution in any medium, provided the original work is properly cited, the use is non-commercial and no modifications or adaptations are made.

© 2025 The Author(s). *Greenhouse Gases: Science and Technology* published by Society of Chemical Industry and John Wiley & Sons Ltd.

a denser phase [2, 6]. These pressure and temperature conditions occur around 800 m in depth below the surface in normal geologic settings but can be highly variable based on local temperature and pressure gradients. CCS projects have been implemented in a diverse array of geologic systems, including offshore [7, 8] and onshore [9, 10] basins but not in geologic fold-and-thrust belts.

1.1 | Fold-and-Thrust Belt CCS Opportunity

Fold-and-thrust belts are a widespread geologic system that may contain hydrocarbon resources, host facilities that emit large quantities of CO_2, and geologic structures that are suitable for trapping large volumes of fluid. However, fold-and-thrust belt systems are rarely studied in the context of carbon storage, presenting a potentially undervalued and overlooked storage opportunity. Collisional tectonics generate fold-and-thrust belts through compressional deformation of pre-orogenic sediments [11, 12]. This deformation causes faulting and folding often creating stacked and/or imbricate structures. Fold structures may act as subsurface topographic highs for fluid accumulation, whereas faults may act as low-permeability seals leading to fluid trapping or high-permeability conduits allowing migration of petroleum charge from source to reservoir [13–17]. As a result, fold-and-thrust belts contain significant hydrocarbon resources in many parts of the world, including the Canadian Cordillera [18–20], the Appalachian Valley and Ridge [21–23], the Zagros belt [24–27], the Atlas belt [28–31], and the Sub-Andes [32–35]. Some estimates suggest that 14%–25% of global hydrocarbon reserves may lie in fold-and-thrust belts, accounting for as much as 710 billion barrels of oil equivalent (BBOE) in discovered reserves [36, 37]. The presence of these significant hydrocarbon reserves is illustrative of the capabilities of fold-and-thrust systems to sequester large volumes of fluids in the subsurface, a capability that could be utilized for carbon storage. Furthermore, analysis of global CO_2 emissions from the Emissions Database for Global Atmospheric Research (EDGAR) indicates that 1.8 billion metric tonnes of CO_2 were emitted in fold-and-thrust belt regions in 2021 [38]. Therefore, fold-and-thrust belt areas could benefit from carbon storage as a means for reducing the CO_2 emissions of these regions. However, to date, there have been no commercial carbon storage projects in fold-and-thrust belts globally. This study investigates large-scale opportunities, for example, known reservoirs and high storage capacities, and limitations, for example, geologic complexity, critically stressed systems, and pressure management, for CCS within fold-and-thrust belt geologic systems to lay the groundwork for future site-specific studies of individual fields.

1.2 | Objectives

The combination of widespread distribution, known geologic reservoirs from hydrocarbon exploration, suitable geometries for structural and stratigraphic trapping, and significant CO_2 emissions make fold-and-thrust belts a promising location for CCS development. The main impediments to CCS in fold-and-thrust belts are the complexity of the geologies, critically stressed systems, and the difficulty in acquiring seismic reflection data, which compound the common challenges to all CCS projects, such as maintaining injectivity, managing pressure, and induced seismicity. The goal of this study is therefore to elucidate the potential of fold-and-thrust belts to securely store commercial-scale volumes of CO_2, that is, millions of tonnes, through computational simulation of three fold-and-thrust play types. These play types describe three geometries common to fold-and-thrust belts globally and include (1) **thrust-ramp** systems involving a medium-to-high-dipping open aquifer; (2) **duplex** systems involving stacked or imbricate faulting resulting in a highly compartmentalized reservoir; and (3) **thrust-fold** systems where folding creates structural traps for fluid and may be dissected by faults that are transmissive or barriers to fluid flow. To ensure that the simulations used in this study are applicable to real geologies, the models developed for each play type are based on well-characterized study sites selected from fold-and-thrust belts. The three sites used for each respective play type are as follows: (1) the Pulaski thrust footwall in Virginia, USA, in the fold-and-thrust Appalachians; (2) the Wilburton field in Oklahoma, USA, in the fold-and-thrust Ouachita belt; and (3) the Incahuasi field in Bolivia in the fold-and-thrust Sub-Andes of South America (Figure 1). Each study site is discretized into a numerical mesh geomodel based on published and interpreted geometries for that site. Simulations of CO_2 injections are run for each site using the TOUGH3 code for non-isothermal multiphase flow in a CO_2–water–NaCl system.

2 | Methods

The three fields selected for this study were chosen on the basis of their characteristic fold-and-thrust geometries and access to subsurface data with which to construct geomodels, such as formation geometries, thicknesses, and rock properties (permeability and porosity). The Pulaski thrust thrust-ramp field was selected because of the authors' involvement with ongoing site characterization work for CCS project development in the area. The Wilburton duplex and Incahuasi thrust-fold fields are both petroleum fields selected due to abundant subsurface data being available through academic publications. The purpose of this study is **not** to suggest CCS development at these specific locations but to use these well-characterized systems as type localities for each CO_2 storage play type (Table 1).

2.1 | Code Selection

For this study, model meshes were constructed using the graphical mesh generator in PetraSim [39] and CO_2 injections were simulated using the TOUGH3 code [40] with the ECO2N v2.0 module for non-isothermal multiphase flow of water, CO_2, and NaCl [41, 42]. The TOUGH3 code utilizes an integral finite volume method in space and a first-order finite difference method in time to solve the mass and energy conservation equations. Phase partitioning is determined on the basis of the local thermodynamic equilibrium.

Rock properties were assigned on the basis of published literature values for the Pulaski thrust [23], Wilburton [43–46], and Incahuasi fields [47] and from well log and core data of the 2500 exploratory well in the Pulaski site (Figure 3) (Table 2). Van Genuchten relative permeability and capillary pressure models were used to account for the multiphase effects of free-phase CO_2 and brine occupying the same pore space [48]. These

21523878, 0, Downloaded from https://scijournals.onlinelibrary.wiley.com/doi/10.1002/ghg.2365 by Virginia Polytechnic Institute, Wiley Online Library on [14/08/2025]. See the Terms and Conditions (https://onlinelibrary.wiley.com/terms-and-conditions) on Wiley Online Library for rules of use; OA articles are governed by the applicable Creative Commons License

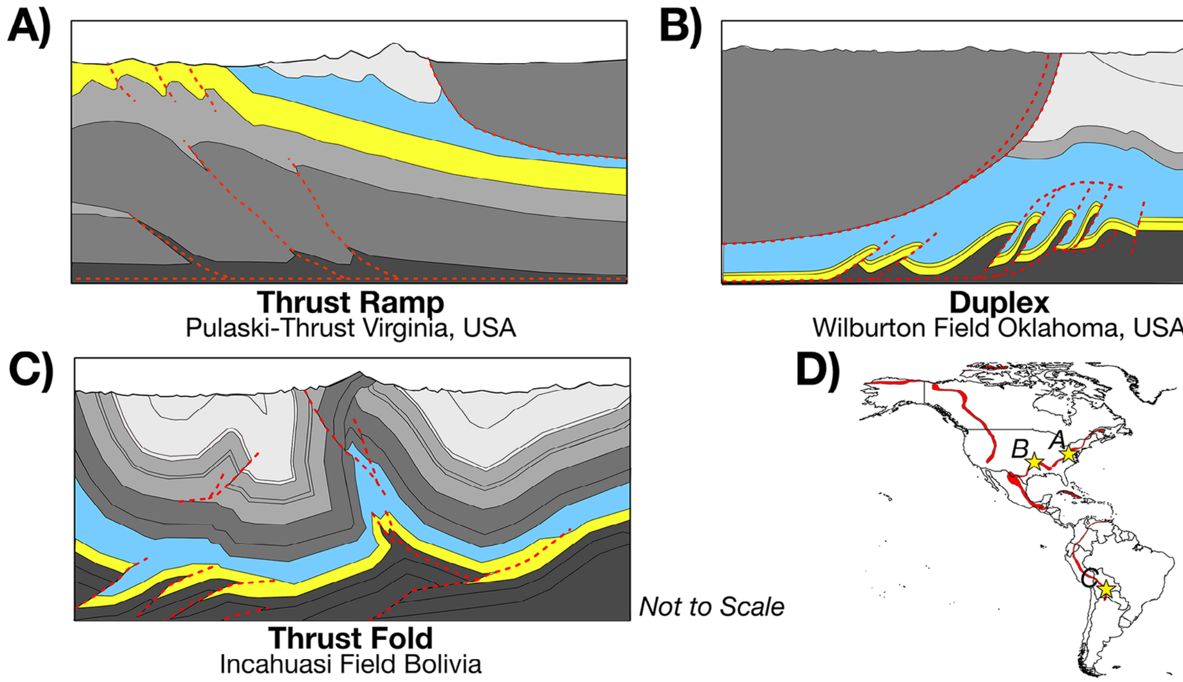

FIGURE 1 | Characteristic cross sections of the three fold-and-thrust play types investigated in this study. Target reservoir formations are shown in yellow; seal formations are shown in blue; other geologic formations are shown in gray; and mapped faults are shown as dashed red lines. Panel A displays the Pulaski thrust footwall's **thrust-ramp**-type geology. Panel B shows the **duplex** structure of the Wilburton field. Panel C shows the fault-dissected **thrust-fold** of the Incahuasi field. Panel D displays the location of these characteristic fields in the Appalachian, Ouachita, and Subandes fold-and-thrust belts.

TABLE 1 | Study matrix describing the three play types and associated study sites used in this study.

Play type	Study site	Operational parameters studied	Trapping mechanisms studied
Thrust-ramp	Pulaski thrust, VA, USA	Storage security in an open system	Hydrodynamic trapping and plume stabilization
Duplex	Wilburton field, OK, USA	Pre-injection fluid production	CO_2 storage density in a pressure-reduced reservoir
Thrust-fold	Incahuasi field, Bolivia	Optimal well placement	CO_2 storage density and pressure buildup along zones of weakness

Note: Operational parameters refer to the aspects of a CCS project that may be controlled by the operator such as selecting a hydraulically open or closed reservoir, conducting formation fluid production, and injection well placement. Trapping mechanisms refers to the phenomena that were investigated for each play type using numerical simulations.

TABLE 2 | Permeability and porosity values for the CO_2 storage reservoirs used in the geomodels for each study site.

Study site	Formation	Permeability (m^2)	Porosity
Pulaski thrust, VA, USA	DSu sandstones	1.45×10^{-14}	0.12–0.16
Wilburton field, OK, USA	Spiro sandstone	1.00×10^{-13}	0.15
Incahuasi field, Bolivia	Huamampampa sandstone	5.00×10^{-14}	0.05

formulations provide a family of characteristic functions in which relative permeability and capillary pressure vary as a function of wetting-phase saturation. These functions are fit to laboratory measurements of sediment parameters like endpoint saturation values. In the absence of CO_2 multiphase rock property data for any of the study sites, this study uses relative permeability and capillary pressure curves for sandstone formation reservoirs from previous studies [40]. Pressure and temperature gradients were determined using surface and well measurements calibrated to hydrostatic equilibrium in each model prior to CO_2 injection [49–53]. Constant pressure and temperature boundaries are then imposed across the top and lateral extent of the model domain to maintain constant fluid pressure at the surface and the far-field pressure and temperature gradients. The site-specific rock property, temperature, and pressure conditions for each model are listed below (Section 2.2).

21523878, 0, Downloaded from https://scijournals.onlinelibrary.wiley.com/doi/10.1002/ghg.2365 by Virginia Polytechnic Institute, Wiley Online Library on [14/08/2025]. See the Terms and Conditions (https://onlinelibrary.wiley.com/terms-and-conditions) on Wiley Online Library for rules of use; OA articles are governed by the applicable Creative Commons License

2.2 | Site Characterization, Geomodel, and CO_2 Storage Scenarios

2.2.1 | Thrust-Ramp Play Type—Pulaski Thrust Footwall, Virginia, USA

The Appalachian Mountains of the eastern United States were primarily formed by three successive orogenic events: the Late Ordovician Taconic orogeny, followed by the Devonian Acadian orogeny, and finally by the Carboniferous (Pennsylvanian) to Permian Alleghenian orogeny [54–56]. The fold-and-thrust belt region of the Appalachians, also known as the Valley and Ridge or Eastern Overthrust province, is defined by the area between the Blue Ridge fault to the east, which displaces crystalline rock of the Appalachian metamorphic core, and the Allegheny Front to the west, which marks the beginning of the Appalachian Basin. The Appalachian Basin has historically been very productive for fossil fuels, especially coal and natural gas [21, 57]. This extensive coal and petroleum extraction as well as adjacent industrial plants involve numerous facilities with large CO_2 emissions, which could benefit from CCS development.

The authors, with support from the Southeast Regional CO_2 Utilization and Storage Acceleration Partnership (SECARB USA), selected the Pulaski thrust footwall as a potential storage site based on its proximity to several CO_2-producing, difficult-to-abate industrial facilities, for example, cement and steel manufacturing, and the likely presence of a reservoir-seal system for storing CO_2. The Pulaski thrust emplaces the Cambrian carbonate rocks of the Catawba Syncline, a doubly plunging synclinal structure, over younger Mississippian and Devonian units [58–60]. There may be additional blind thrusting and associated deformation in the Pulaski thrust footwall and below or west of the Catawba Syncline. This study site is generally representative of the central and southern Appalachian fold-and-thrust belt as it contains a larger regional fold (Catawba Syncline) and thrust system (Pulaski thrust) that may be compartmentalized further by minor faults and folds (potential blind thrusting in the Pulaski footwall) developed on intermediate detachment (shale) horizons. The proposed CO_2 storage complex targets Siluro-Devonian sandstone units (DSu) that have been previously identified as potential CCS reservoirs, including the Oriskany sandstone, the Keefer/Eagle Rock sandstone, and the Tuscarora sandstone, which are overlain by the Millboro shale seal [61]. The structure of the Pulaski footwall dips to the southeast creating a "ramp-type" geometry in the storage complex, with the target reservoirs reaching a depth of about 3050 m (10,000 ft) below the surface at the proposed injection site beneath the Catawba Syncline and outcropping at the surface about 20 km to the northeast (Figure 2). This presents a challenge for carbon storage security as buoyant injected CO_2 is likely to move up-dip. A simulation study was conducted in order to assess the likelihood of leakage due to CO_2 migration under three kinematically feasible structural models [62]. The Koehn et al. study showed that with favorable geologic properties, the capillary force needed to drain brine from the reservoir may exceed the buoyancy force of the CO_2 prior to the CO_2 plume migrating to the surface, resulting in secure storage [62]. The study also demonstrated how fold-and-thrust structures may act as traps, accumulating injected CO_2 and mitigating up-dip flow.

The evidence for feasibility provided by Koehn et al. [62] led to partner support for a ~762 m (2500 ft) shallow borehole to acquire core and assess rock properties in the up-dip shallow portion of the study site (Figure 3). Core analysis indicates that the borehole passed through about 106 m (350 ft) of Millboro shale, followed by the entire Siluro-Devonian interval, which was found to be 365 m (1200 ft) thick in the study site, and the upper 290 m (950 ft) of the Ordovician interval (Figure 5). Core observation and density logs suggest that there is >10% porosity in several sandstone formations of the Siluro-Devonian interval, totaling ~126 m (415 ft) thickness of potential high-porosity reservoir for a net-to-gross ratio of 0.28 in the DSu. Analysis also suggested that there may be porous intervals in the sandstones and limestones of the Upper Ordovician interval that may be utilized as secondary reservoir for CO_2 storage. Further evidence for these porous intervals comes from gamma ray and NPHI logs from a 1981 exploratory well drilled by Columbia Natural Resources LLC. This well was drilled up to 9300 ft measured depth near Eagle Rock, VA (northeast of the Pulaski footwall location but within comparable geology) completing in what is thought to be the Upper Ordovician interval [63]. It is not possible to correlate the individual porous sandstone sections, the shallow borehole discussed here, and the Columbia well at this time; however, the Columbia well provides evidence for porosity within the DSu and Ou sections at depths of 6000–9000 ft, suggesting that the porosity observed in the shallow 2500 ft borehole may be preserved at the depths proposed for injection in this model [63].

The thickness and porosity of formations from the borehole were used to update the models from Koehn et al. (Figure 4) [62]. The model was also further refined from ~400,000 grid cells in the original model to ~2,100,000 grid cells, resulting in smaller grid cell volume and a reduction in numerical dispersion error. The model domain is 15.7 km by 11.3 km with a maximum ground surface elevation of 960 m above mean sea level (msl), an average surface elevation of ~400 m above msl, and a depth of 3300 m below msl. Grid cell area ranges from 200 m^2 near the injection point to 18,000 m^2 in the far field. Grid cells are discretized in the vertical dimension by 11 m between 0 and 2750 m msl. Vertical grid cell discretization is 220 m per cell above and below this interval. The model includes a single injection well with completions in the DSu interval at depths of 2054–2138 and 2233–2328 m below msl, which is 2465–2549 and 2644–2739 in measured depth (MD). Reservoir permeability (DSu interval) is 1.45×10^{-14} m^2 (14.7 md) based on permeability measurements in the Devonian Oriskany sandstone at the Bergton gas field north of the study site [23]. Reservoir (DSu interval) porosity is divided into a low-porosity zone (<10%) and a high-porosity zone (12%–16%) based on core description and logs from the borehole (Figure 3). Initial pressure gradients were assigned on the basis of the hydrostatic pressure gradient of a brine with 100,000 ppm, which is within the range of salinity values for brines within the Siluro-Devonian interval at the depths tested here [64, 65], and then calibrated for variations in surface elevation, resulting in pressures of ~26–29 MPa in the target reservoir interval. Temperature gradients were calculated in the model using a surface temperature of 15°C and regional heat flow measurements and then calibrated to equilibrium [50]. This results in an average temperature gradient of 0.02°C/m.

21523878, 0, Downloaded from https://scijournals.onlinelibrary.wiley.com/doi/10.1002/ghg.2365 by Virginia Polytechnic Institute, Wiley Online Library on [14/08/2025]. See the Terms and Conditions (https://onlinelibrary.wiley.com/terms-and-conditions) on Wiley Online Library for rules of use; OA articles are governed by the applicable Creative Commons License

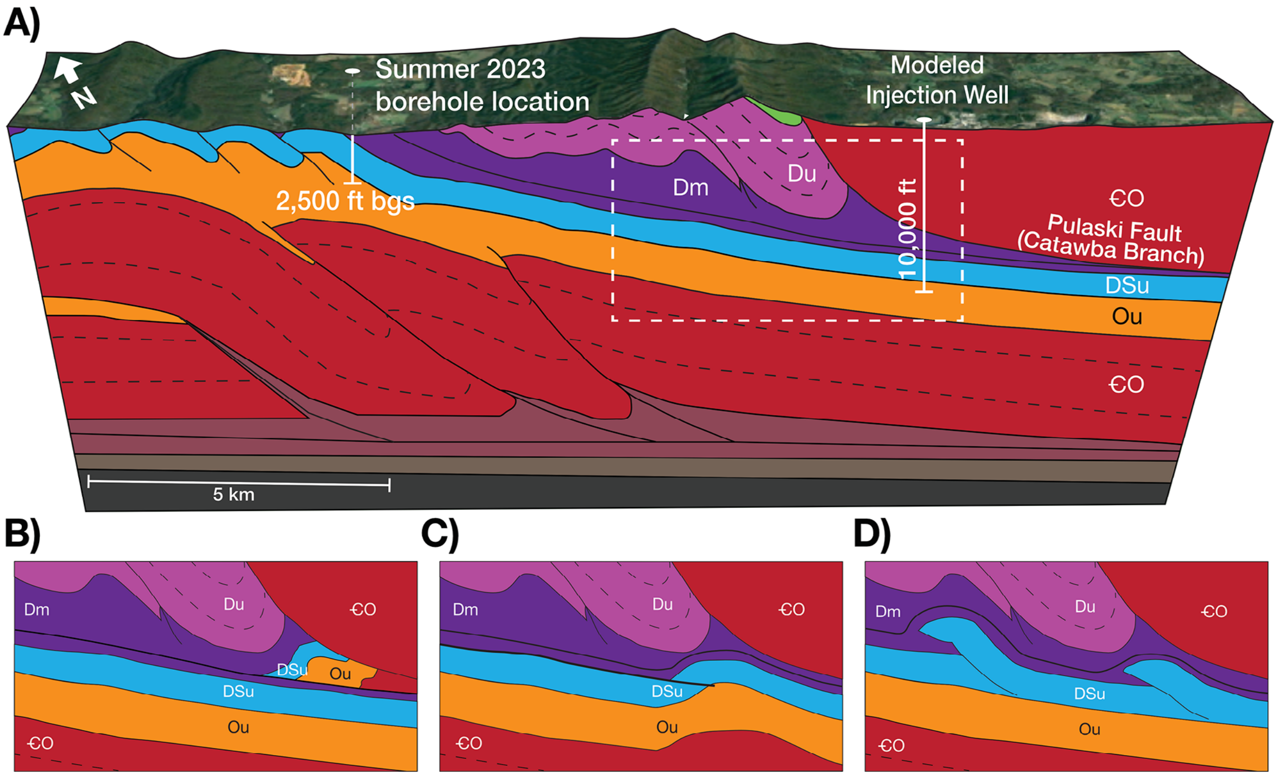

FIGURE 2 | Kinematically feasible cross-section interpretations of the Pulaski thrust footwall study site. The Mississippian Price formation is shown in green. The pink Du interval represents shale and sandstone Upper Devonian formations. The purple Dm formation represents the Millboro shale, which is the primary seal for this study and the glide horizon for the Pulaski thrust fault. The blue DSu formation represents the Siluro-Devonian interval, which includes the target sandstone reservoirs. The orange Ou interval represents the Upper Ordovician sandstone, shale, and limestone formations. The red € O formation represents Ordovician and Cambrian carbonates and basement rock. Panel A represents a geology with no blind thrusting. Panel B represents a geology where DSu and Ou units have been displaced by the Pulaski thrust forming horse blocks. These horse blocks do not alter the CO_2 storage complex but may present drilling challenges. Panels C and D represent different thrust faulting scenarios with detachment occurring in either the € O (Panel C) or Dm (Panel D) interval.

The injection scenario for this play type comprises a constant rate injection of 1.7 million metric tonnes CO_2 per year for 30 years, resulting in ~50 million metric tonnes of CO_2 injected, followed by simulation of the postinjection period to assess long-term storage security. This injection rate was determined on the basis of the US Department of Energy requirements for a CarbonSAFE initiative project, that is, a minimum injection of 50 million tonnes CO_2 over 30 years [66]. This model uses a single injection well with a constant rate; however, injection rates in an implemented CCS project may be limited by mechanical and borehole constraints requiring additional injection wells or different injection strategies. The simulation is run using the updated model with structural scenario A (Figure 2A) to further test whether this type of fold-and-thrust structure, that is, a thrust-ramp reservoir that outcrops at the surface, may be viable for commercial-scale carbon storage.

2.2.2 | Duplex Play Type—Wilburton Field, Oklahoma, USA

The Ouachita orogeny of the southern United States began in the Carboniferous (Pennsylvanian) period and is generally equivalent to the Alleghanian orogeny of the Appalachians [56, 67, 68]. The Ouachita Mountains form major outcrops in Arkansas and Oklahoma and have generated associated foreland basins such as the Arkoma, Ardmore, and Anadarko basins. There are significant petroleum resources in both the Ouachita Mountains themselves [69, 70] and the associated basins [71, 72]. One petroleum field in the frontal Ouachitas, that is, the fold-and-thrust belt separating the core of the Ouachita Mountains from the foredeep basin, is the Wilburton gas field in southwestern Oklahoma.

The Wilburton field is a triangle zone structure bound by the Carbon fault to the north and the Choctaw fault to the south [73, 74]. The structure is a triangle zone or passive duplex where the roof fault of the duplex features backthrust relative to the imbricate thrust faults forming the limbs or “horse blocks” of the duplex and the general direction of deformation from the formation of the fold-and-thrust belt [75, 76]. In short, the roof thrust of the duplex is opposite of the general direction of thrusting, creating the structural trap that has held petroleum in the Wilburton field and may be viable for carbon storage. Over 250 bcf of natural gas has been trapped in the Spiro sandstone reservoir, which is thrusted and segmented by the duplex structure (Figure 5) [73]. The duplex is bound by the Woodford and Springer detachments which form in the Upper Devonian Woodford shale and the Mississippian Springer shale,

21523878, 0, Downloaded from https://scijournals.onlinelibrary.wiley.com/doi/10.1002/ghg.2365 by Virginia Polytechnic Institute, Wiley Online Library on [14/08/2025]. See the Terms and Conditions (https://onlinelibrary.wiley.com/terms-and-conditions) on Wiley Online Library for rules of use; OA articles are governed by the applicable Creative Commons License

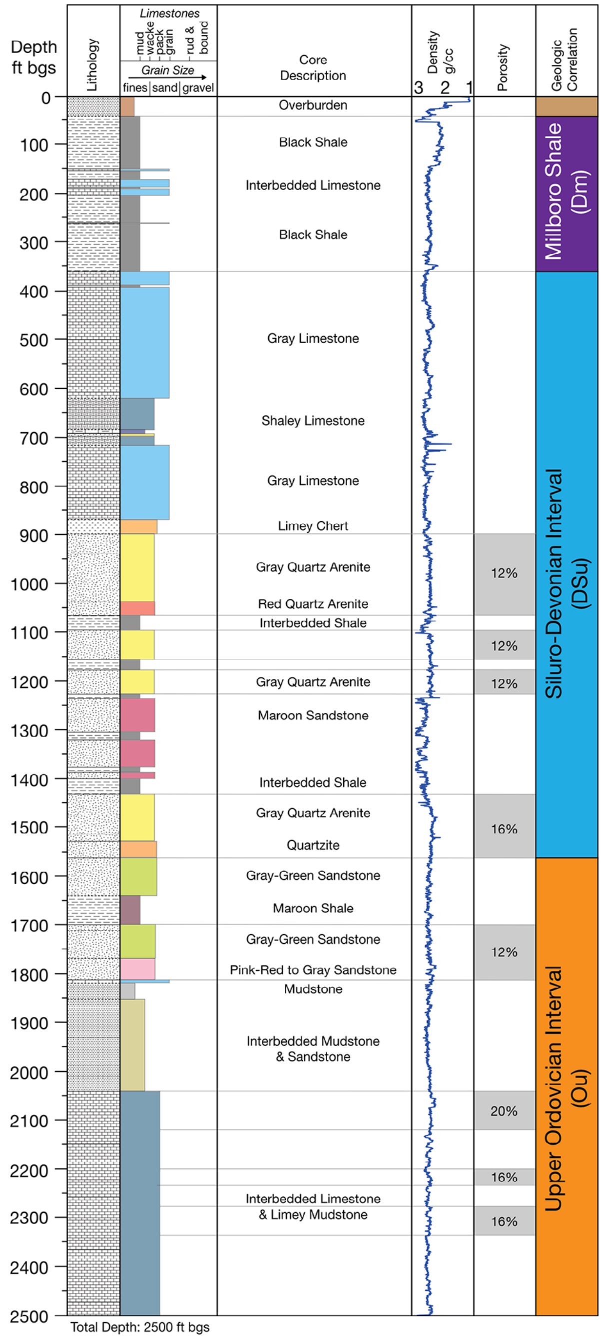

FIGURE 3 | Core description, density log, and interpreted porosity for the Pulaski thrust borehole. The high-porosity formations in the Siluro-Devonian interval are the target reservoirs for this site, with the overlying Millboro formation acting as the primary seal.

respectively. The Spiro sandstone is the lowermost member of the Pennsylvanian Atoka formation and a major petroleum reservoir in the Arkoma basin and Ouachita petroleum systems [69, 77]. The Spiro is immediately overlain by a shale member of the Middle Atoka formation which acts as a sealing unit [73, 74]. As the duplex has been heavily penetrated by petroleum wells, it may be a difficult site for future CCS development; however, the abundant subsurface data can be used to construct a model of the system to better understand how carbon storage may behave in this and other duplex structures. Therefore, we are not proposing CCS development at the Wilburton field; rather, this study uses the Wilburton site to assess whether duplex structures, which are bounded by both low-permeability faults and sealing layers, can accommodate commercial volumes of injected CO_2 without overpressuring the reservoir and risking containment loss due to induced fracturing, fault dilation, and/or induced seismicity.

The model domain for this site was constructed on the basis of interpreted cross sections, well logs, and formation tops from Hepner [73] and Akhtar [74] (Figure 5). It includes ~650,000 grid cells and is 8.2 km by 6.5 km with a maximum ground surface elevation of 422 m above msl, an average surface elevation of ~100 m above msl, and a depth of 4400 m below msl. Grid cell area ranges from 20 m^2 near the injection point to 10,000 m^2 in the far field. Grid cells are discretized in the vertical dimension by 26 m between 540 m below msl and −3940 m below msl. Vertical grid cell discretization is 90 m per cell above and below this interval. Reservoir permeability (Spiro sandstone) is 1.00×10^{-13} m^2 (101.3 md), and porosity is 15% based on average literature values [43–46]. Initial pressure gradients were assigned on the basis of the hydrostatic pressure gradient of a brine with 100,000 ppm, which is within the range of salinities for the Mississippian–Pennsylvanian formations in the Ouachita thrust-belt and Arkoma basin at the depths tested here [64] and then calibrated for variations in surface elevation. Temperature gradients were calculated in the model using a surface temperature of 15°C and regional heat flow measurements and then calibrated to equilibrium [50]. This results in an average temperature gradient of 0.02°C/m.

The injection scenario utilizes three injection wells, one in each of the limbs of the duplex structure. Well 1 in the westernmost limb is completed at depths of 3400–3450 m below msl (3546–3596 m MD), Well 2 in the middle limb is completed at depths of 3325–3375 m below msl (3453–3503 m MD), and Well 3 in the easternmost limb is completed at depths of 3145–3195 m below msl (3250–3300 m MD) (Figure 5B). All three wells target the Spiro sandstone on the down-dip limb of the duplexed formation. The simulation suite for this Wilburton site comprises six simulations testing a combination of injection strategies and initial pressure conditions. All six simulations involve a constant pressure injection of CO_2 simultaneously in the three injection wells for a period of 30 years. In the first two simulations, the reservoir is hydrostatically pressured, and injection occurs at constant rates of 0.5 and 2.0 MPa over the hydrostatic pressure for each well. This results in injection pressures of about 37.5–38.1, 36.8–37.3, and 34.9–35.4 MPa in the 0.5 MPa injection and about 39.0–39.6, 38.3–38.8, and 36.4–36.9 MPa in the 2.0 MPa injection pressure scenario for Wells 1, 2, and 3, respectively. As past simulation studies have shown that producing brine pre- and syn-injection significantly reduces pressure in the reservoir and may allow for more secure storage of CO_2 [8, 78, 79], in the following scenarios, the reservoir is pressure depleted to 10 MPa representing a scenario where significant hydrocarbon or brine production has occurred. Simulations are conducted with constant pressure injections of 0.5 and 2.0 MPa over the newly depleted pressure (10.5 and 12.0 MPa injection pressures) and at the same rates as the hydrostatic pressure scenario (35–40 MPa injection pressures).

21523878, 0, Downloaded from https://scijournals.onlinelibrary.wiley.com/doi/10.1002/ghg.2365 by Virginia Polytechnic Institute, Wiley Online Library on [14/08/2025]. See the Terms and Conditions (https://onlinelibrary.wiley.com/terms-and-conditions) on Wiley Online Library for rules of use; OA articles are governed by the applicable Creative Commons License

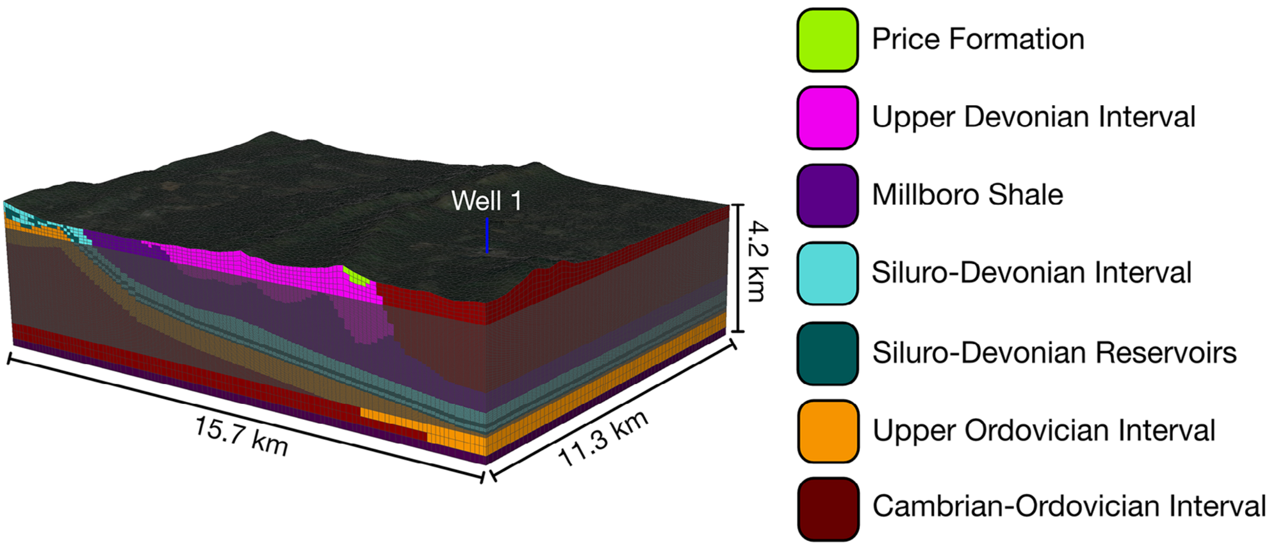

FIGURE 4 | Geomodel for the Pulaski thrust footwall and Catawba Syncline. High-porosity formations within the Siluro-Devonian interval are discretized and displayed as dark blue.

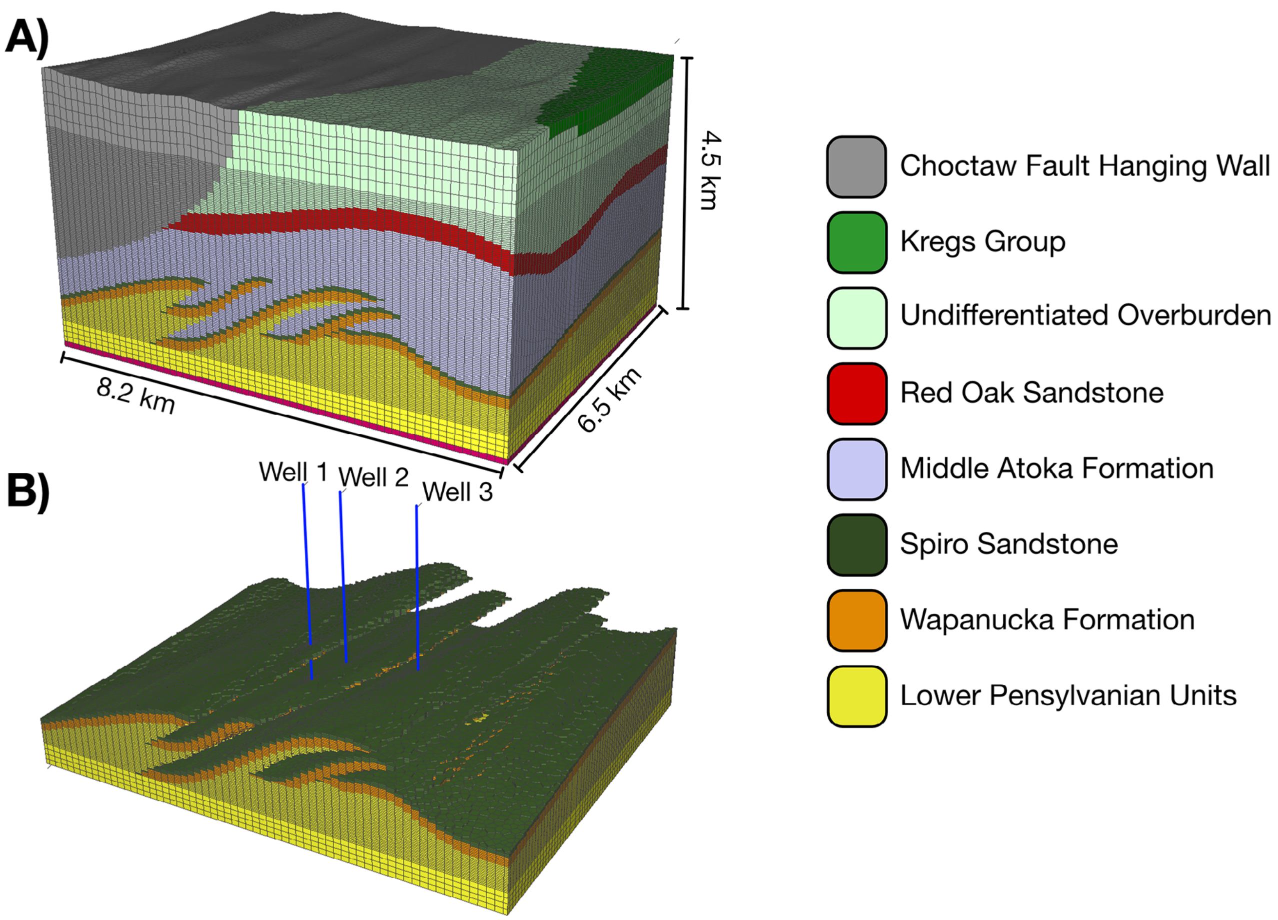

FIGURE 5 | Geomodel for the Wilburton gas field study site. The three modeled injection wells are completed within the Spiro sandstone near the base of each of the three duplex arms. Panel A depicts the entire model domain, whereas Panel B depicts only the Spiro sandstone reservoir and underlying units, displaying the 3D geometry of the duplex structure.

21523878, 0, Downloaded from https://scijournals.onlinelibrary.wiley.com/doi/10.1002/ghg.2365 by Virginia Polytechnic Institute, Wiley Online Library on [14/08/2025]. See the Terms and Conditions (https://onlinelibrary.wiley.com/terms-and-conditions) on Wiley Online Library for rules of use; OA articles are governed by the applicable Creative Commons License

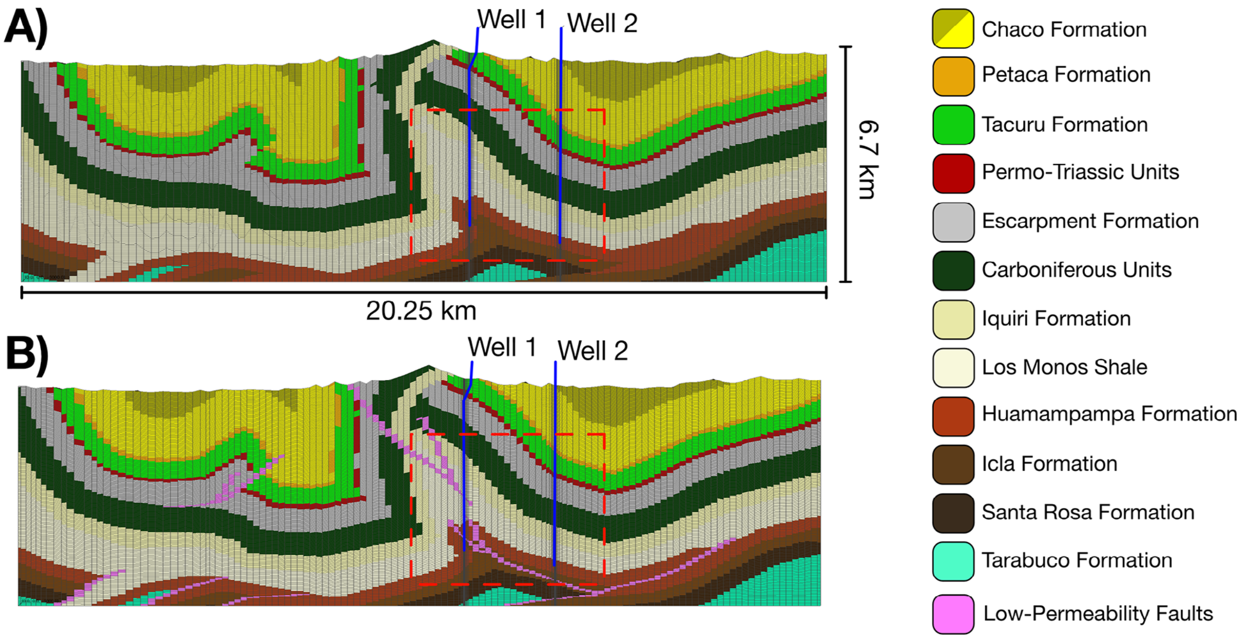

FIGURE 6 | Geomodel for the Incahuasi study site. Structural geometry is constant in the out-of-plane direction. Well 1 is the approximate location of the existing production well. Well 2 is a simulated CO_2 injection well targeting the limb of the Incahuasi fold in order to access greater storage volume for CO_2. Panel A depicts the model scenario where faults are transmissive and likely will not impair CO_2 flow. Panel B depicts the model scenario where faults act as low-permeability barriers to flow due to accumulated fault gouge, which may limit the accessible storage volume for CO_2 injection where the Huamampampa formation is dissected by faults. The red box indicates the location of the simulation results shown in Figure 8.

2.2.3 | Thrust-Fold Play Type—Incahuasi Field, Bolivia

The Andes Mountains of South America were formed by the subduction of the oceanic Nazca plate under the South American plate during the Mesozoic-Cenozoic eras [80]. The Andes orogeny has also created an extensive foreland basin system to the west of the mountain range [81]. The Andean fold-and-thrust belt system, also known as the Sub-Andes, contains significant petroleum resources in countries such as Bolivia and Argentina. Specifically, the southern Bolivian Sub-Andes may contain over fifty tcf of natural gas reserves, with several "giant fields" (>500 MMboe or >3.0 tcf natural gas) located in Devonian-aged reservoirs [33, 35].

One such giant gas field was discovered by Total and Tecpetrol in 2004 and named the Incahuasi field [34]. The reservoir at Incahuasi is the Devonian Huamampampa sandstone formation, which is overlain by the Los Monos, a thick (>600 m) shale that acts as a regional seal and source rock for hydrocarbons [82]. The Incahuasi field features a large thrust fault-driven anticline which is bisected by two sets of faults near the gas accumulation (Figure 6). The upper thrust fault set originates in the Los Monos shale and breaches the surface, whereas the lower fault set cuts through and deforms the Huamampampa and the underlying Icla, Santa Rosa, and Tarabuco formations [34]. This site is an excellent example of thrust faulting and associated folding combining to form a trap that allows for major fluid, in this case natural gas, accumulation. As there is ongoing active production in the field and the reservoirs are quite deep, >3000 m, this field is not an ideal location for CCS development. However, this field was selected for model development in this study as seismic and drilling data allow us to more accurately model the geologic system and its response to CCS injection. Therefore, we are using this less than ideal, but well-characterized, field to study the general storage parameters of **thrust-fold** structures so that learnings may be applied to similar structures elsewhere in fold-and-thrust belts. Multiple CCS injection scenarios for this study site are considered to determine optimal well placement for maximizing storage efficiency while minimizing pressure buildup in fold-and-thrust structures.

The model domain for this site was constructed on the basis of the 2D cross-section interpretation of seismic reflection and drilling data from Heidmann et al. projected into the 3D plane (Figure 6) [34]. The model domain includes ~1,700,000 grid cells and is 20.25 km by 10 km with a maximum ground surface elevation of 1724 m above mean sea level (amsl), an average surface elevation of ~1000 m above msl, and a depth of 5000 m below msl. Grid cell area ranges from 20 m^2 near the injection point to 20,000 m^2 in the far field. Vertical grid cell discretization is 31.50 m per cell throughout the model. Reservoir permeability (Huamampampa formation) is 5.00×10^{-14} m^2 (50.7 md), and porosity is 5% based on literature values [47]. Initial pressure gradients were assigned on the basis of the hydrostatic pressure gradient of a brine with 100,000 ppm, which, in the absence of site-specific salinity data for this field, was used to maintain consistency with the other two models tested in this study, and then calibrated for variations in surface elevation. Initial temperature gradients were calculated in the model using measurements from nearby deep drilling [51, 52] and regional heat flow measurements [53] and then calibrated to equilibrium. This results in an average temperature gradient of 0.025°C/m.

The injection scenario comprises four simulations, testing two well placements with two end-member fault permeability scenarios each. Well 1 repurposes the existing petroleum production well to a CO_2 injection well near the crest of the antiform structure

21523878, 0, Downloaded from https://scijournals.onlinelibrary.wiley.com/doi/10.1002/ghg.2365 by Virginia Polytechnic Institute, Wiley Online Library on [14/08/2025]. See the Terms and Conditions (https://onlinelibrary.wiley.com/terms-and-conditions) on Wiley Online Library for rules of use; OA articles are governed by the applicable Creative Commons License

with a completion depth of 3332–3352 m below msl (4672–4692 m MD) in the Huamampampa reservoir (Figure 6). This well placement represents the conventional well placement strategy at the structural high for conventional petroleum resource extraction. Well 2 is a hypothetical well targeting the limb of the fold with a completion depth of 3860–3880 m below msl (5008–5028 m MD), also within the Huamampampa reservoir, representing a CCS-minded placement designed to increase total storage capacity (Figure 6). For both well placements, simulations are conducted in which the thrust faults act as low-permeability barriers to flow and in which the faults are transmissive conduits for flow to test what affect the faults may have on the overall storage performance of the system. Each simulation was run for 30 years of CO_2 injection at a constant pressure of 0.5 MPa over the initial pressure, 48.0 and 50.3 MPa for Wells 1 and 2, respectively.

3 | Results and Discussion

3.1 | Storage Security in Thrust-Ramp Architecture

Simulation results provide further evidence that the Pulaski thrust footwall is a viable CCS site for securely storing commercial volumes of CO_2. As in Koehn et al. [62], the simulated CO_2 plume remains securely stored in the reservoir without migrating to surface (Figure 7). The CO_2 plume at the end of the 30-year injection period is 2965 by 3147 m in diameter and has a maximum column height of 928 m with two lobes concentrated in the high-porosity injection intervals that were identified in the characterization borehole. The simulation was then run an additional 1000 years with no injection to assess the leakage risk from up-dip migration of the CO_2 plume. After the 1000-year period, the CO_2 plume stabilized and ceased migration while remaining in the target DSu interval in a supercritical phase, thus achieving secure storage during the 1000-year simulation. The resulting stable CO_2 plume is approximately 7031 by 5240 m in diameter, reached a minimum depth of 1125 m below msl, has a maximum column height of 32 m, and is about 5490 m from outcropping at the surface. The injection also creates an increase in pore fluid pressure (ΔP_f) which is 4057 by 3167 m in diameter with a maximum ΔP_f of about 3 MPa (435 psi), resulting in a pressure of ∼32 MPa (4640 psi) at the point of injection. Assuming an average rock fracture gradient of 15.8 kPa/m (0.7 psi/ft), the fracture pressure at the interval of injection is 39–43 MPa; therefore, this injection scenario remains below the EPA Class VI requirement to not exceed 90% of the rock fracture pressure during injection.

These results provide further evidence that thrust-ramp-type geologic structures are capable of storing commercial volumes of injected CO_2 without a structural trap. Loss of CO_2 containment is a concern for CCS at this location due to the lack of structural trap and dipping open reservoir, which may allow significant CO_2 plume migration in the up-dip direction towards the reservoir outcrop at the surface. However, in the simulation case, the geology successfully stored 50 million tonnes of CO_2 using solubility and capillary trapping to stabilize and retard CO_2 plume migration, keeping the entirety of injected CO_2 below the surface at depths suitable for storing CO_2 in the supercritical phase. In this case, the open reservoir allows for rapid accommodation of injection pressure during and post-CO_2 injection, resulting in less engineered pressure driving CO_2 migration. The plume does migrate up-dip as a result of CO_2 buoyancy; however, as the CO_2 plume disperses and dissolves into formation brine, the total buoyancy force decreases until it is no longer sufficient to drive drainage or displacement of formation brine in the reservoir, resulting in stabilization of the CO_2 plume due to hydrodynamic forces.

Furthermore, the CO_2 plume migrates and spreads laterally within the open reservoir, the surface area of contact between supercritical CO_2 and formation brines increases, resulting in very high rates of CO_2 dissolution, known as solubility trapping. During the injection period, about 7.4 million metric tonnes of CO_2 dissolves into formation brine representing 14.8% of the total injected CO_2, but even greater dissolution occurs in the postinjection period, resulting in 30.4 million metric tonnes of cumulative CO_2 dissolved at the time of plume stabilization for 60.8% of the total injected CO_2. As CO_2-saturated brine is denser than in situ brine, the saturated brine sinks to the bottom of the reservoir thus removing the risk of up-dip CO_2 leakage for the dissolved CO_2 resulting in secure permanent carbon sequestration. These results suggest that commercial volumes of carbon storage may be permanently sequestered in thrust-ramp geometries that lack structural traps. This play type of CCS results in a larger lateral project area than projects with structural traps, which would require a significant pore space leasing position; however, the play type also facilitates significant solubility trapping pulling CO_2 into the aqueous phase where it is nonmobile and permanently stored.

3.2 | Maximizing Storage and Minimizing Risk in Closed Duplex Systems

Simulation results from the Wilburton model demonstrate the challenges of storing CO_2 in closed pressure systems while also demonstrating how brine production may open additional opportunities for commercial-scale carbon storage, especially in fold-and-thrust structures, like the Wilburton duplex (Table 3).

Under hydrostatic pressure conditions, rapid injection-driven pressure accumulation within the closed aquifer of the duplex system acts as a limit on both total CO_2 injection volume and injection rate under a constant pressure injection strategy. Extracting brine from the aquifer may decrease the initial pressure and therefore allow for greater volumes of CO_2 to be injected. However, as pressure in the reservoir decreases, so too does the density of stored CO_2 resulting in a less dense and therefore less efficient storage system. For example, at reservoir conditions of 80°C and 32.0 MPa, CO_2 has a density of 763.36 kg/m^3, whereas at reservoir conditions of 80°C and 12.0 MPa, CO_2 has a density of 303.68 kg/m^3 [83]. Operationally, this would mean the same volume of injected gas occupies more pore space in lower pressured reservoirs compared to higher pressured reservoirs, hence the lower volumes of injected CO_2 in our model simulation results when injecting at 10.5 and 12.0 MPa. Additionally, altering reservoir pressure will result in changes to other thermodynamic properties of the CO_2-brine system, as lower pressures result in lower dynamic viscosities, lower specific heat capacities, and higher interfacial tension contributing to

21523878, 0, Downloaded from https://scijournals.onlinelibrary.wiley.com/doi/10.1002/ghg.2365 by Virginia Polytechnic Institute, Wiley Online Library on [14/08/2025]. See the Terms and Conditions (https://onlinelibrary.wiley.com/terms-and-conditions) on Wiley Online Library for rules of use; OA articles are governed by the applicable Creative Commons License

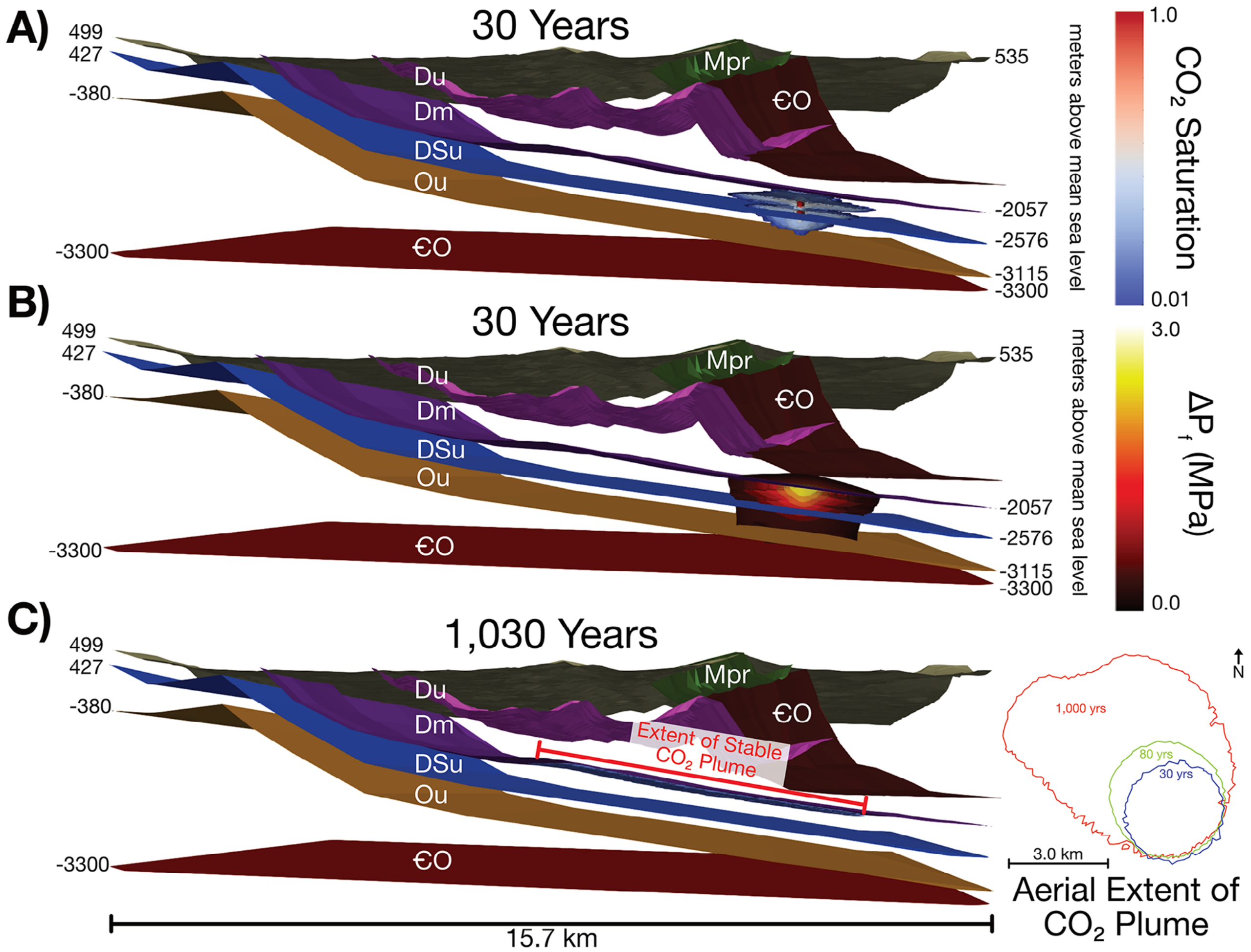

FIGURE 7 | Simulation results displaying CO_2 (Panel A) and fluid pressure (ΔP_f) (Panel B) plumes at the conclusion of the 30-year injection period and at full stabilization of the CO_2 plume at 1030 years postinjection (Panel C). The injected CO_2 plume forms a cone shape during the injection period but migrates up-dip and flattens against the overlying seal unit postinjection resulting in a laterally extensive, but very thin plume. The maximum increase in fluid pressure (ΔP_f) is 3 MPa near the injection well and decreases laterally away from the injection well. Also shown is the aerial extent of the CO_2 plumes at 30, 80, and 1000 years since injection began (0, 50, and 9970 years postinjection, respectively).

TABLE 3 | Summary of simulation results demonstrating the various storage capacities of the closed duplex system based on geologic pressure conditions and operating parameters (injection pressures).

	Total CO_2 stored (MMt)	
Approximate injection pressure (MPa)	**Hydrostatic reservoir pressure: ~34–38 MPa**	**Depleted reservoir pressure: ~10 MPa**
10.5	X	0.094
12.0	X	4.9
34.9–38.1	3.6	30.9
36.4–39.6	20.0	98.9

Note: MMt is million metric tonnes of CO_2.

reduced brine displacement and CO_2 flow [83, 84]. Lowering the reservoir fluid pressure through brine extraction may also allow operators to inject at higher bottomhole pressures with reduced risk of fracturing the reservoir. This strategy, injecting at ~>35 MPa against an initial pressure of 10.0 MPa, achieves the greatest injected CO_2 volumes in our study (Table 3). This injection strategy also results in the greatest change in reservoir temperature across the simulations. Injecting CO_2 into a reservoir tends to result in cooling of the reservoir near the injection well due to Joule-Thomson cooling from CO_2 expansion as well as heating of the reservoir due to heat release from CO_2 dissolution into formation brine [85]. Injecting against hydrostatic pressure results in a maximum temperature decrease of −0.8°C near the injection wells and maximum temperature increase of 1.4°C away

21523878, 0, Downloaded from https://scijournals.onlinelibrary.wiley.com/doi/10.1002/ghg.2365 by Virginia Polytechnic Institute, Wiley Online Library on [14/08/2025]. See the Terms and Conditions (https://onlinelibrary.wiley.com/terms-and-conditions) on Wiley Online Library for rules of use; OA articles are governed by the applicable Creative Commons License

from the well. Injecting at >35 MPa against a reduced reservoir pressure results in significant cooling of the system as the injected CO_2 has greater pressure space to expand. This strategy results in a maximum temperature decrease of −8°C near the injection wells with a minimum decrease of −0.35°C and no temperature increase anywhere in the reservoir. A temperature decrease from 82°C to 74°C in the reservoir is unlikely to significantly alter the mechanical properties of the rock but may have minor impacts on the stress–strain state of the formation resulting in changes to properties such as permeability and porosity. Geomechanical changes in reservoir properties such as porosity and permeability in response to pressure and temperature changes, such as matrix compaction, may also play a role in total storage capacity and injectivity of CCS projects but are not considered in these simulations. Furthermore, reducing reservoir pressure by ~25 MPa and then quickly repressurizing it through CO_2 injection may not be technically or economically feasible for many fields; however, these simulations provide possible end-member demonstrations of how variations in reservoir pressure affect the storage properties of a formation, that is, pressure-depleted reservoirs have reduced storage capacities relative to hydrostatically pressured reservoirs unless repressurized significantly, as a result of changes in the density of the injected CO_2 and the effects on the interfacial tension within the pore space.

The injection strategies tested here utilize constant pressure injections; however, past studies on water injection have suggested that a gradual rate ramp-up during injection may reduce risks related to induced seismicity on critically stressed faults [86, 87]. Conley et al. [86] found that a linear ramp-up injection rate results in a more gradual pressure buildup compared to other ramp-up strategies or a constant maximum rate strategy, such as those used in this study. However, the maximum pressure increase is not affected by ramp-up strategy and is dependent on the maximum injection rate. For CCS within duplexes and other closed structures, a gradual ramp-up of injection rate and pressures would assist in reducing geomechanical failure risks, which is especially important in a closed system where pressure buildup is a concern.

Injecting at lower bottomhole pressures, 10.5 and 12.0 MPa in our study, reduces the energy cost of injection and therefore may be desirable for smaller injection volume commercial projects depending on the specific economic context of the project. For CCS projects targeting tens of millions of tonnes CO_2 injection, a closed duplex system such as the Wilburton field would require significant fluid production to produce the pressure space and storage capacity needed to hit those injection targets. Therefore, the closed-aquifer duplex play type is more suitable for smaller injection volume CCS projects.

3.3 | Optimal Well Placement and Storage Security in Fold-and-Thrust Structures

Results from four Incahuasi study site simulations demonstrate how optimizing well placement for CCS by targeting the down-dip leg of fold-and-thrust structures increases storage capacity and reduces risks associated with caprock integrity. Key results from each simulation include the volume of CO_2 injected and the increase in fluid pressure on the crest of the antiform structure

TABLE 4 | Key results from simulation suite of the Incahuasi site.

	CO_2 (MMt)		ΔP_f (MPa)	
	High k fault	**Low k fault**	**High k fault**	**Low k fault**
Well 1	11.2	6.8	0.83	3.67
Well 2	36.6	17.7	2.26	3.42

Note: MMt is million metric tonnes of CO_2 stored. ΔP_f is the maximum increase in pore fluid pressure at the crest of the antiform fold in megapascals (MPa). Regarding the faults, k is permeability, where high k faults have permeabilities of 5.00×10^{-14} m^2 and low k faults have permeabilities of 1.00×10^{-17} m^2.

where the overlying Los Monos shale seal is mechanically weakest. These results are outlined in Table 4, and the extent of the CO_2 plume is illustrated in Figure 8.

Well placement 2 on the limb of the fold results in greater CO_2 injection volumes compared to well placement 1 on the crest of the antiform as the placement increases the storage capacity of the system for CO_2 by targeting the fetch volume rather than the accumulation point at the crest. This is consistent with Nicot and Hovorka [88] and Bump and Hovorka [89, 90], who proposed repurposing term "fetch," which refers to the volume available for a petroleum source that migrates to the petroleum reservoir, for CCS as the volume of reservoir available for storing CO_2, including buoyant up-dip flow. Using this CCS-minded well placement to increase the fetch volume for storage results in CO_2 storage volumes 2.6–3.3 times greater than the hydrocarbon-minded well placement. This well placement also reduces fluid pressure accumulation at the crest of the fold per volume of stored CO_2. As the crest of a fold is often the mechanically weakest section of the overlying seal unit, minimizing pressure buildup at this area of weakness improves the storage security of the system. With well placement 1, the simulation stores 11.2 MMt of CO_2 for 0.83 MPa of pressure buildup on the fold crest resulting in a pressure increase of 74.11 kPa per MMt of CO_2. Well placement 2 utilizes a larger storage volume to hold 36.6 MMt with 2.26 MPa pressure buildup on the crest resulting in a pressure increase of 61.75 kPa per MMt of CO_2 stored. Moreover, as previously discussed regarding the Wilburton field, a more gradual pressure buildup has been shown to reduce geomechanical failure risks [87]. With well placement 2, pressure accumulates along the crest of the fold more gradually as CO_2 migrates up-dip from the injection point, likely further improving storage security compared to well placement 1 near the crest of the fold. Therefore, the CCS-minded well placement results in less mechanical stress placed on the seal unit from fluid pressure per stored volume of CO_2, resulting in more secure storage for the same volumes of storage compared to a hydrocarbon-minded well placement.

These results also demonstrate how low-transmissibility sealing faults pose a challenge to CCS in fold-and-thrust belts as they may impede CO_2 and brine flow resulting in high accumulated fluid pressures and lower accessible storage volume. This accumulated pressure at the crest of the fold and along the fault in low-permeability scenarios may result in mechanical failure of the sealing unit, induced seismic activity, fault dilation, shear offset, and aseismic stress transfer, all of which pose risks to the successful operation of a CCS project [91]. Risks associated with

21523878, 0, Downloaded from https://scijournals.onlinelibrary.wiley.com/doi/10.1002/ghg.2365 by Virginia Polytechnic Institute, Wiley Online Library on [14/08/2025]. See the Terms and Conditions (https://onlinelibrary.wiley.com/terms-and-conditions) on Wiley Online Library for rules of use; OA articles are governed by the applicable Creative Commons License

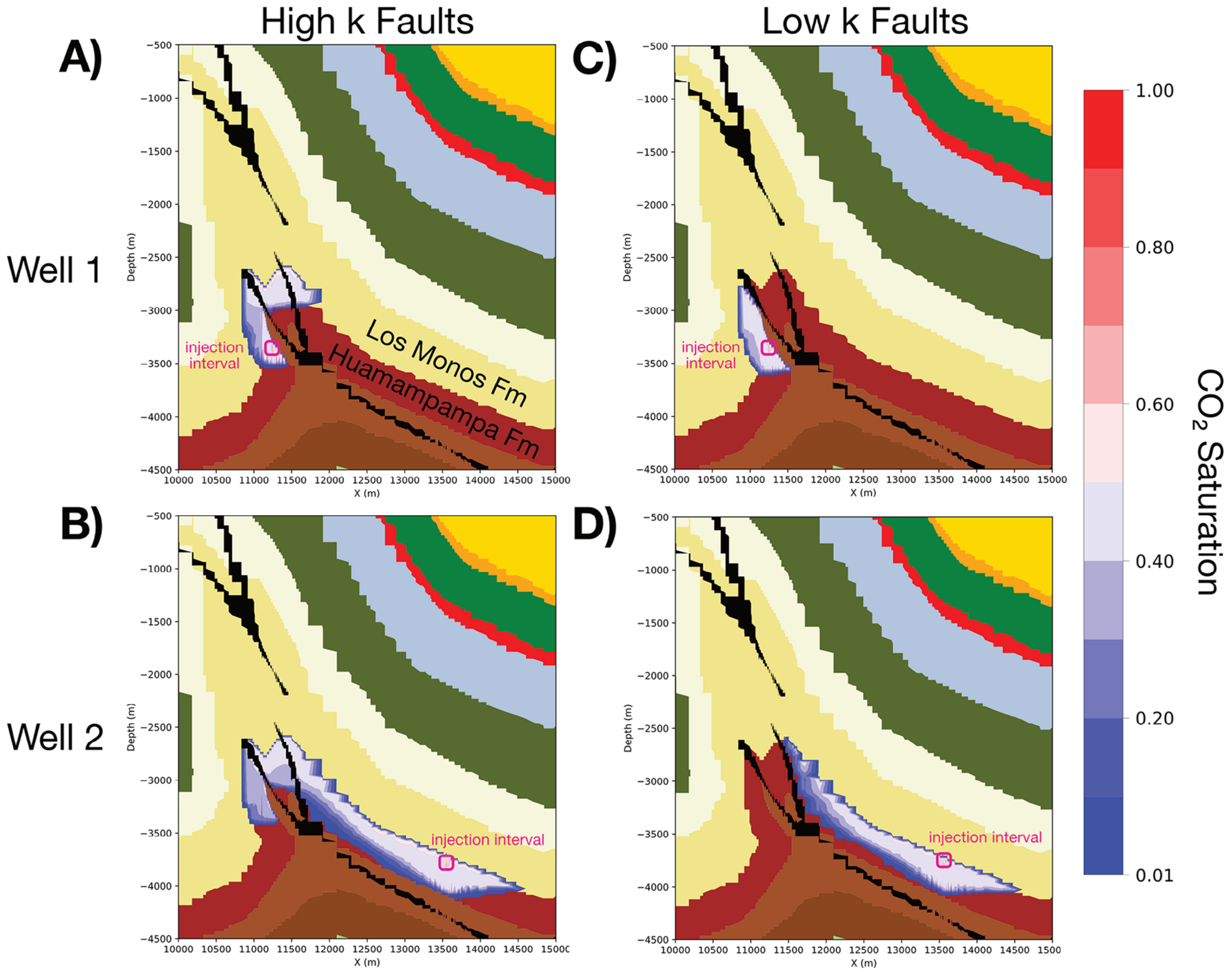

FIGURE 8 | Simulation results from the Incahuasi model illustrating the effect of well placement and fault permeability on the CO_2 trapping characteristics of the system. The target reservoir Huamampampa formation is shown in maroon, the primary seal Los Monos Formation is shown in beige, and low-permeability faults are shown in black. Panel A displays the scenario with well placement 1 and transmissive faults, Panel B displays the model scenario with transmissive faults and well placement 2, Panel C displays the model scenario with well placement 1 and sealing faults, and Panel D displays the model scenario with well placement 2 and sealing faults. Panel B achieves the greatest total storage of CO_2 at 36.6 MMt as the single injector well is able to access the majority of the storage (pore space) accessible to CO_2 in the fold trap. Other scenarios achieve lower storage volumes as the well placement (Panels A and C) or sealing faults (Panels C and D) prevent access to some part of the reservoir.

induced seismicity are a significant concern for these projects and are thus further discussed in detail below (Section 3.4). Overall, the simulation results from the Incahuasi model demonstrate how CCS-minded well placement can maximize CO_2 storage capacity by increasing fetch volume and reducing mechanical failure risks and that the large fold architectures common to fold-and-thrust belts may be capable of storing commercial volumes of injected CO_2.

3.4 | Injection-Induced Geomechanical Risks

Industrial-scale carbon storage requires CO_2 fluid to be injected underground at high pressure, which affects the original mechanical equilibrium state of the reservoir and surrounding rocks. Previous studies suggest that large-scale fluid injections into deep geologic formations can trigger unintended seismic activity [92–96]. The Mohr-Coulomb theory explains the connection between fluid injections and induced seismic activity, asserting that heightened pore fluid pressure correlates with a decrease in effective normal stress on a fault [95, 97, 98]. This theory remains valid even when factoring in poroelastic relaxation effects [99]. As fluids are injected into the subsurface, pore fluid pressure plumes spread away from the injection point, commonly known as fluid pressure propagation or injection-induced fluid pressure transients [97, 100, 101]. In CCS projects, these injection-induced fluid pressure transients are expected to propagate faster and farther than the injected CO_2 plume, increasing the area that needs to be assessed for seismic risks [85, 102]. If an injection-generated fluid pressure transient intersects a preexisting fault that is both critically stressed and optimally oriented with the regional stress field, unintended earthquakes may occur. When fluid pressure transients interact with a preexisting fault, they cause a decrease in effective normal stress, thereby reducing the shear strength of the fault. This reduction in shear strength can potentially lead to induced seismicity when the fault slips [95, 97, 98].

21523878, 0, Downloaded from https://scijournals.onlinelibrary.wiley.com/doi/10.1002/ghg.2365 by Virginia Polytechnic Institute, Wiley Online Library on [14/08/2025]. See the Terms and Conditions (https://onlinelibrary.wiley.com/terms-and-conditions) on Wiley Online Library for rules of use; OA articles are governed by the applicable Creative Commons License

To date, the recorded seismic activity resulting from CO_2 injection has predominantly consisted of microseismic events and occasional felt tremors [103]. Due to the absence of significant earthquakes, seismicity has not posed a major issue for CCS projects thus far. However, despite the lack of significant earthquakes, the potential for induced seismicity remains a sizable hazard that requires attention to mitigate future instances and repercussions. The consequences of fault reactivation and induced seismicity can manifest in four primary scenarios: property damage, contamination of drinking water with brine or CO_2, and public nuisance [103–106]. These scenarios not only directly affect the well-being of communities in the vicinity of the project but can also jeopardize the long-term viability of CCS operations. Large-scale CCS operations must evaluate all possible modes of failure that could jeopardize project viability, including induced seismicity. For instance, the In Salah project, situated at the gas-producing Krechba field in Algeria, serves as a noteworthy case study. Here, CO_2 injections resulted in a total of 9506 microseismic events, with a maximum moment magnitude (Mw) of 1.7 [107]. The event rate closely followed the CO_2 injection rate. Consequently, the In Salah project was suspended in June of 2011.

The geomechanical response to CO_2 injection varies depending on the geologic setting [108]. Unlike In Salah, which operated within a foreland basin, the projects under consideration in this research are situated within fold-and-thrust belts. As such, it is imperative to account for the distinct geological characteristics of fold-and-thrust belts and the possible structural elements that could contribute to instances of CO_2 injection-induced seismic events. Fold-and-thrust belt settings are characterized by strong deformation, where subsurface structures are incredibly complex and include faults, repeating stratigraphy, and steeply dipping to overturned strata [109]. Within fold-and-thrust belts, a diverse array of faults exists, encompassing various types, characteristics, and orientations. Two common fault types are high-angle thrust faults and faults linked to local disturbances like intrusions [110]. Additionally, faults may be confined to strata or basement rock or cut through both layers. Due to the history of deformation, faults within fold-and-thrust belts are likely to be critically stressed, and in the case where faults remain critically stressed and optimally oriented to the regional stress field, they present a major risk for induced seismicity [95, 97, 98]. Faults within a CCS project site must be evaluated relative to the regional stress field in order to properly characterize the risks associated with injection-induced seismicity.

Recent instances of induced seismicity in the Appalachian Basin—linked to activities such as wastewater disposal and hydraulic fracturing—offer valuable insights into seismic risks in the locations investigated for this study. With a surge in natural gas production from the Marcellus shale play in Pennsylvania and West Virginia, there has been a corresponding increase in the need to dispose of large volumes of wastewater [111]. This wastewater was shipped to eastern Ohio and injected underground in Cambrian, Ordovician, and Silurian dolomites and sandstones [112–114]. These injections coincided with an increase in seismicity rates from 2010 onwards, including an ML 4.0 in Youngstown, Ohio, USA [111]. Furthermore, hydraulic fracturing operations in Harrison County, Ohio, generated a series of seismic sequences between 2013 and 2017, with magnitudes not exceeding M_L 2.8 [115]. These events occurred in the basin near the proposed CCS site in the Pulaski Thrust Footwall used in this study and thus shed light on operational practices that could exacerbate the risks of CO_2 injection-induced earthquakes within fold-and-thrust belts and further emphasize the need to constrain the extent and magnitude of fluid pressure transients into the subsurface surrounding injection wells.

Accidental hydraulic fracturing of the reservoir rock is another risk for CO_2 projects that must be managed during the operation of a commercial project. Current US Environmental Protection Agency (EPA) Class VI CO_2 injection requirements require CO_2 injections to remain below the fracture pressure of the reservoir rock [116]. This requirement acts as a limit on the injection pressure and rate for CO_2 injections to ensure that the operator does not unintentionally create fractures in the reservoir or sealing formation that may allow CO_2 to leak to the surface or contaminate groundwater. In formations with low permeability and therefore low injectivity or in closed systems where pressure may accumulate rapidly, such as the duplex play type investigated in this study, this requirement presents a limit for storing large volumes of injected CO_2. Producing reservoir fluid, such as brine or hydrocarbons, may reduce pressure buildup in the reservoir to allow for CO_2 injection; however, this creates additional challenges such as the added cost of production wells, accidental production of injected CO_2, and produced brine disposal which then requires its own waste disposal injection in an alternate formation which may lead to induced seismic events as discussed in the previous paragraph. Plampin et al. [117] proposed that brine production and reinjection into formations overlying and underlying the Mt. Simon sandstone in the Illinois basin, which is currently being utilized as a CO_2 storage reservoir by the Decatur CCS project, could increase CO_2 injectivity by over one million tonnes per year [10, 117]. Economic and seismic risk tradeoffs should be performed on a site-specific basis for each CCS project to determine if brine production is viable at that site.

4 | Conclusions

This study presents multiphase fluid flow simulations to evaluate the trapping characteristics of geologic fold-and-thrust belts. We define three general play types, the thrust-ramp, duplex, and thrust-fold plays that appear suitable for commercial-scale carbon storage. Numerical investigations of these play types using geomodels of a prospective CCS project and two well-characterized petroleum fields demonstrate that these plays may facilitate the storage of millions of tonnes of CO_2 in fold-and-thrust belt regions. These results define large-scale performance attributes for fold-and-thrust systems that may open the door for future site-scale investigations of these regions for CCS potential. Specifically, we find

1. The **thrust-ramp play type** may securely store millions of tonnes of CO_2 despite the lack of a structural trap using hydrodynamic and solubility trapping under suitable reservoir conditions over a 1000-year period. Projects of this play type will likely require an extensive pore-space ownership position due to the lateral and up-dip migration of CO_2 observed in the simulation; however, this play type also results in high, 60+%, percentages of injected CO_2 being dissolved in formation brine resulting in secure storage. Therefore, this play type

21523878, 0, Downloaded from https://scijournals.onlinelibrary.wiley.com/doi/10.1002/ghg.2365 by Virginia Polytechnic Institute, Wiley Online Library on [14/08/2025]. See the Terms and Conditions (https://onlinelibrary.wiley.com/terms-and-conditions) on Wiley Online Library for rules of use; OA articles are governed by the applicable Creative Commons License

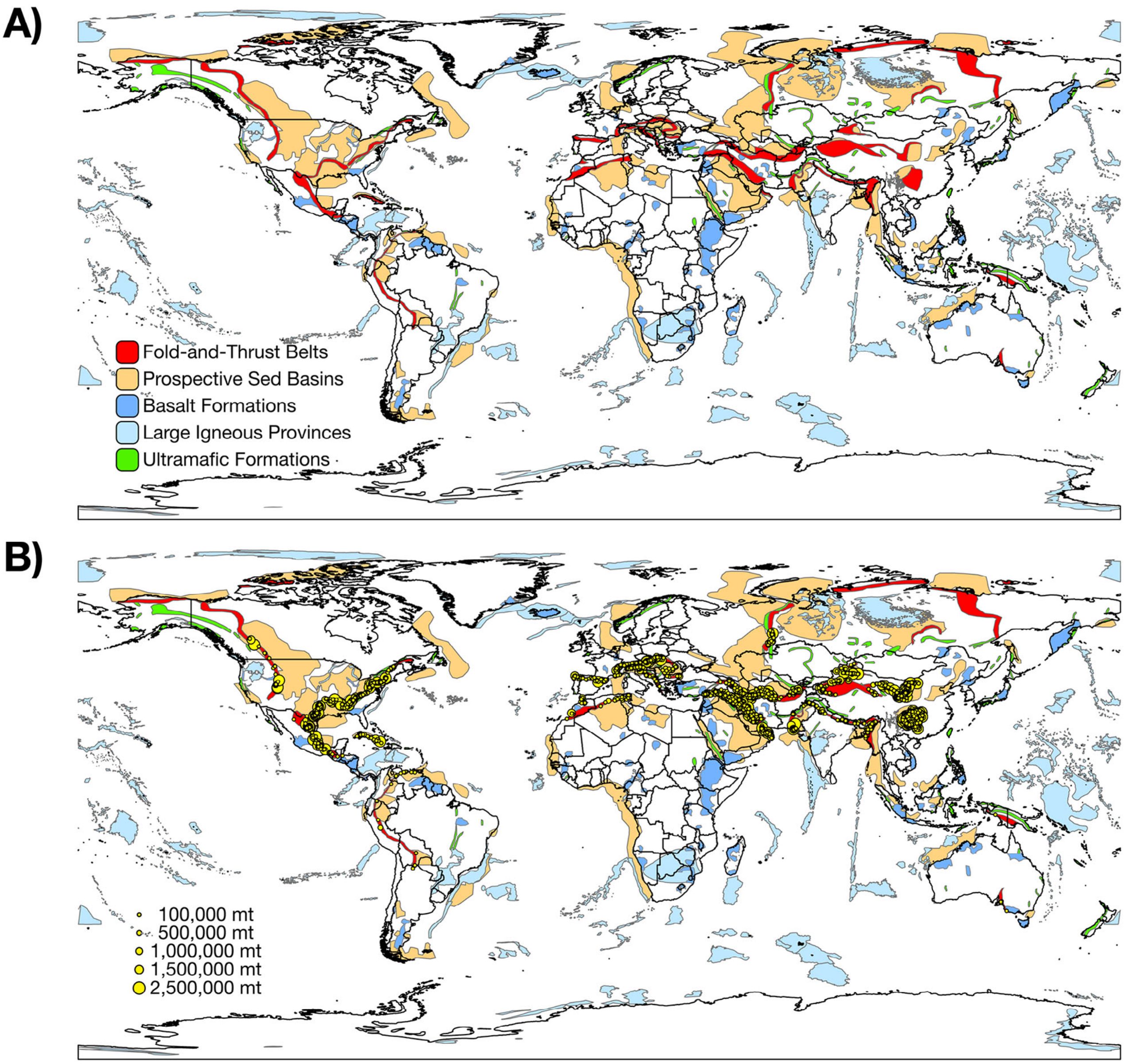

FIGURE 9 | Global map (Panel A) of geologic carbons storage opportunities, including sedimentary storage (basins and fold-and-thrust belts) and mineralization storage (basalt formations, large igneous provinces, and ultramafic formations). Panel B displays CO_2 emission sources greater than 100,000 metric tonnes (mt) per year that occur within fold-and-thrust belt geologies presenting a 1.8 Gt carbon storage opportunity. *Source:* Sedimentary basins highly prospective for CO2 storage adapted from Bradshaw and Dance [3]; basalt and ultramafic formations adapted from Kelemen et al. [4]; large igneous provinces from Coffin et al. [118]; fold-and-thrust belts adapted from Goffey et al. 2010 [119]; and CO_2 emissions data from EDGAR 2022 [38].

is most suitable for regions where subsurface ownership positions are low-cost or easy to obtain.

2. The **duplex play type** may be suitable for CO_2 storage under naturally pressured conditions, but the total storage of the system is limited due to fluid pressure buildup in the closed duplex trap. Brine or petroleum production may lower the pressure in the reservoir and allow for greater quantities of CO_2 injection; however, this introduces additional challenges and costs for production wells and wastewater disposal. Additionally, lowering reservoir pressure reduces the storage density of CO_2 affecting the overall capacity of the system for carbon storage. Duplexes, therefore, may be viable for smaller volume commercial CCS projects and larger volume projects assisted by fluid production depending on the economic context of individual projects.

3. The **thrust-fold play type** presents the most straightforward opportunity for commercial CCS in fold-and-thrust belts as CCS-minded well placement to maximize fetch volume may unlock two to three times greater storage capacity in these systems compared to conventional hydrocarbon-minded well placement. Additionally, as fold-and-thrust belts frequently feature complex faulting and folding, faults that dissect the target storage reservoirs may reduce the accessible storage capacity per well. Careful characterization of faults and their sealing properties is therefore necessary for instances where faulting intersects the storage complex.

21523878, 0, Downloaded from https://scijournals.onlinelibrary.wiley.com/doi/10.1002/ghg.2365 by Virginia Polytechnic Institute, Wiley Online Library on [14/08/2025]. See the Terms and Conditions (https://onlinelibrary.wiley.com/terms-and-conditions) on Wiley Online Library for rules of use; OA articles are governed by the applicable Creative Commons License

Globally, there are an estimated 1.8 Gt of CO_2 emitted in fold-and-thrust belt regions annually, including emissions related to petroleum resources and difficult-to-abate industries such as cement and steel production, which could benefit from carbon storage implementation [38]. Fold-and-thrust belts with significant emissions include the Appalachian-Ouachita belt in the Eastern and Southern United States, the Zagros belt in the Middle East, the Alps and Carpathian belts in Europe, and the Circum-Sichuan and Tarim belts in China (Figure 9).

The regulatory and economic environment for CCS and CO_2 transport pipelines is complex and challenging with several recent proposed CO_2 pipelines in the United States being cancelled [120–122]. Therefore, it may be advantageous for CO_2 source operators in fold-and-thrust belts to develop carbon storage projects adjacent to their existing facilities within fold-and-thrust geologies rather than to attempt to transport the CO_2 to other areas. This study defines and proposes three fold-and-thrust play types, the thrust-ramp, duplex, and thrust-fold, which may facilitate the storage of millions of tonnes of CO_2 within fold-and-thrust geologic structures.

Acknowledgments

This material is based upon work supported by the Department of Energy under Award Number DE-FE0031830 through the Southeast Regional Carbon Sequestration Partnership, which is managed by the Southern States Energy Board under contract #SSEB-SECARBUSA-931-VAT-2020. This manuscript was prepared as an account of work sponsored by an agency of the US Government. Neither the US Government nor any agency thereof, nor any of their employees, makes any warranty, express or implied, or assumes any legal liability or responsibility for the accuracy, completeness, or usefulness of any information, apparatus, product, or process disclosed, or represents that its use would not infringe privately owned rights. Reference herein to any specific commercial product, process, or service by trade name, trademark, manufacturer, or otherwise does not necessarily constitute or imply its endorsement, recommendation, or favoring by the US Government or any agency thereof. The views and opinions of authors expressed herein do not necessarily state or reflect those of the US Government or any agency thereof.

References

1. IPCC. "Summary for Policymakers," in *Climate Change 2021: The Physical Science Basis Contribution of Working Group I to the Sixth Assesment Report of the Intergovernmental Panel on Climate Change* (Cambridge University Press, 2021), 3–32.

2. S. Bachu, "CO_2 Storage in Geological Media: Role, Means, Status and Barriers to Deployment," *Progress in Energy and Combustion Science* 34 (2008): 254–273.

3. J. Bradshaw and T. Dance, "Mapping Geological Storage Prospectivity of CO_2 for the World Sedimentary Basins and Regional Source to Sink Matching," *Greenhouse Gas Control Technologies* 7 (2005): 583–591, https://doi.org/10.1016/B978-008044704-9/50059-8.

4. P. Kelemen, S. M. Benson, H. Pilorge, P. Psarras, and J. Wilcox, "An Overview of the Status and Challenges of CO_2 Storage in Minerals and Geological Formations," *Frontiers in Climate* 1 (2019): 9.

5. NETL. *Carbon Storage Atlas*, 5th ed. (National Energy Technology Laboratory (NETL), 2015).

6. S. M. Benson and D. R. Cole, "CO_2 Sequestration in Deep Sedimentary Formations," *Elements* 4 (2008): 325–331.

7. A.-K. Furre, O. Eiken, A. Havard, J. N. Vevatne, and A. F. Kiær, "20 Years of Monitoring CO_2 Injection at Sleipner," *Energy Procedia* 114 (2017): 3916–3926.

8. T. A. Buscheck, J. A. White, S. A. Carroll, J. M. Bielicki, and R. D. Aines, "Managing Geologic CO_2 Storage With Pre-Injection Brine Production: A Strategy Evaluated With a Model of CO_2 Injection at Snøhvit," *Energy and Environmental Science* 9 (2016): 1504–1512.

9. L. Rock, S. O'Brien, S. Tessarolo, et al., "The Quest CCS Project: 1st Year Reciew Post Start of Injection," *Energy Procedia* 114 (2017): 5320–5328, https://doi.org/10.1016/j.egypro.2017.03.1654.

10. S. E. Greenberg, R. Bauer, R. Will, et al., "Geologic Carbon Storage at a One Million Tonne Demonstration Project: Lessons Learned From the Illinois Basin—Decatur Project," *Energy Procedia* 114 (2017): 5529–5539, https://doi.org/10.1016/j.egypro.2017.03.1913.

11. J. Poblet and R. J. Lisle, "Kinematic Evolution and Structural Styles of Fold-and-Thrust Belts," *Geological Society of London, Special Publications* 349 (2011): 1–24.

12. D. Roeder, *American and Tethyan Fold-Thrust Belts* (Gebrüder Borntraeger, 2009).

13. S. Mitra, "Fault-Propagation Folds: Geometry, Kinematic Evolution, and Hydrocarbon Traps," *AAPG Bulletin* 74, no. 6 (1990): 921–945, https://doi.org/10.1306/0C9B23CB-1710-11D7-8645000102C1865D.

14. S. Mitra, "Duplex Structures and Imbricate Thrust Systems: Geometry, Structural Position, and Hydrocarbon Potential," *AAPG Bulletin* 70 (1986): 1087–1112, https://doi.org/10.1306/94886A7E-1704-11D7-8645000102C1865D.

15. J. P. Fairley and J. J. Hinds, "Field Observation of Fluid Circulation Patterns in a Normal Fault System," *Geophysical Research Letters* 31, no. 19 (2004): L19502.

16. A. D. Hindle, "Petroleum Migration Pathways and Charge Concentration: A Three-Dimensional Model," *AAPG Bulletin* 81, no. 9 (1997): 1451–1481, https://doi.org/10.1306/3B05BB1E-172A-11D7-8645000102C1865D.

17. D. A. Karlsen and J. E. Skeie, "Petroleum Migration, Faults, and Overpressure, Part I: Calibrating Basin Modelling Using Petroleum in Traps—A Review," *Journal of Petroleum Geology* 29, no. 3 (2006): 227–256, https://doi.org/10.1111/j.1747-5457.2006.00227.x.

18. C. D. Dahlstrom, "Structural Geology of the Eastern Margin of the Canadian Rocky Mountains," *Bulletin of Canadian Petroleum Geology* 18, no. 3 (1970): 332–406.

19. F. G. Fox, "Structure and Accumulation of Hydrocarbons in Southern Foothills, Alberta, Canada," *AAPG Bulletin* 43, no. 5 (1959): 992–1025, https://doi.org/10.1306/0BDA5D05-16BD-11D7-8645000102C1865D.

20. W. B. Gallup, "Geology of Turner Valley Oil and Gas Field, Alberta, Canada," *AAPG Bulletin* 35, no. 4 (1951): 797–821, https://doi.org/10.1306/3D9341ED-16B1-11D7-8645000102C1865D.

21. R. T. Ryder, R. C. Milici, C. S. Swezey, and M. H. Trippi, "Appalachian Basin Oil and Natural Gas: Stratigraphic Framework, Total Petroleum Systems, and Estimated Ultimate Recovery," in *Coal and Petroleum Resources in the Appalachian Basin: Distribution, Geologic Framework, and Geochemical Character*, ed. L. Ruppert and R. Ryder (USGS, 2014), 1–3.

22. R. Ryder and W. A. Zagorski, "Nature, Origin, and Production Characteristics of the Lower Silurian Regional Oil and Gas Accumulation, Central Appalachian Basin, United States," *AAPG Bulletin* 87, no. 5 (2003): 847–872, https://doi.org/10.1306/01210300199.

23. R. S. Young and W. T. Harnsberger, "Geology of Bergton Gas Field," *AAPG Bulletin* 39, no. 3 (1955): 317–328, https://doi.org/10.1306/5CEAE14B-16BB-11D7-8645000102C1865D.

24. M. L. Bordenave and J. A. Hegre, "Current Distribution of Oil and Gas Fields in the Zagros Fold Belt of Iran and Contiguous Offshore as the Result of the Petroleum Systems," in *Tectonic and Stratigraphic Evolution of Zagros and Makran During the Mesozoic–Cenozoic*, ed. P. Leturmy and C. Robin (Geological Society of London, 2010), 291–353.

21523878, 0, Downloaded from https://scijournals.onlinelibrary.wiley.com/doi/10.1002/ghg.2365 by Virginia Polytechnic Institute, Wiley Online Library on [14/08/2025]. See the Terms and Conditions (https://onlinelibrary.wiley.com/terms-and-conditions) on Wiley Online Library for rules of use; OA articles are governed by the applicable Creative Commons License

25. M. L. Bordenave, "The Middle Cretaceous to Early Miocene Petroleum System in the Zagros Domain of Iran, and Its Prospect Evaluation," in *AAPG Annual Meeting* (American Association of Petroleum Geologists, 2002), 1–9.

26. L. Aldega, S. Corrado, E. Carminati, A. Shaban, and S. Sherkati, "Thermal Evolution of the Kuh-e-Asmari and Sim Anticlines in the Zagros Fold-and-Thrust Belt: Implications for Hydrocarbon Generation," *Marine and Petroleum Geology* 57 (2014): 1–13, https://doi.org/10.1016/j.marpetgeo.2014.04.017.

27. Z. R. Beydoun, M. W. H. Clarke, and R. Stonely, "Petroleum in the Zagros Basin: A Late Tertiary Foreland Basin Overprinted Onto the Outer Edge of a Vast Hydrocarbon-Rich Paleozoic-Mesozoic Passive-Margin Shelf," in *Foreland Basins and Fold Belts*, ed. R. W. Macqueen and D. A. Leckie (American Association of Petroleum Geologists, 1992), 9–46.

28. R. Mezni and S. Khomsi, "An Overview of the Eastern Atlas Fold and Thrust Belt and Its Foreland Basin Along the North–South Axis and Chorbane–Ktitir Platform: Surface/Subsurface Major Structures and Tectonic Evolution (North Africa)," in *Geology of North Africa and the Mediterranean: Sedimentary Basins and Georesources*, ed. S. Khomsi and F. Roure (Springer, 2023), 187–243.

29. A. Saïd, P. Baby, D. Chardon, and J. Ouali, "Structure, Paleogeographic Inheritance, and Deformation History of the Southern Atlas Foreland Fold and Thrust Belt of Tunisia," *Tectonics* 30, no. 6 (2011): TC6004, https://doi.org/10.1029/2011TC002862.

30. W. F. Bishop, "Petroleum Geology of East-Central Tunisia," *AAPG Bulletin* 72, no. 9 (1988): 1033–1058.

31. H. E. Euchi, M. Saidi, L. Fourati, and C. El Maherssi, "Northern Tunisia Thrust Belt: Deformation Models and Hydrocarbon Systems," in *Deformation, Fluid Flow, and Reservoir Appraisal in Foreland Fold and Thrust Belts*, ed. R. Swennen, F. Roure, and J. W. Granath (AAPG, 2004), 371–390.

32. M. A. Uliana, M. E. Arteaga, L. Legarreta, J. J. Cerdán, and G. O. Peroni, "Inversion Structures and Hydrocarbon Occurrence in Argentina," *Geological Society of London Special Publications* 88 (1995): 211–233, https://doi.org/10.1144/gsl.sp.1995.088.01.13.

33. F. J. Dunn, K. G. Hartshorn, and P. W. Hartshorn, "Structural Styles and Hydrocarbon Potential of the Sub-Andean Thrust Belt of Southern Bolivia," in *Petroleum Basins of South America*, eds. A. Tankard, R. Soruco, and H. Welsink (AAPG, 1995): 523–544.

34. J.-C. Heidmann, J. Durand, P. Mallard, J.-F. Ballard, and J.-M. Moron, "Discovery of a Bolivian Foothills Giant Gas Field: Incahuasi," in *Giant Fields of the Decade 2000–2010*, eds. R. K. Merrill and C. A. Sternbach (AAPG, 2017), 153–164.

35. F. Fuentes, D. Starck, and E. Rocha, "Geometry and Kinematics of Structures of the Southern Sub-Andean Fold-Thrust Belt of Bolivia," in *Petroleum Basins and Hydrocarbon Potential of the Andes of Peru and Bolivia*, eds. G. Zamora, K. R. McClay, and V. A. Ramos (AAPG, 2018), 443–464.

36. M. Cooper, "Structural Style and Hydrocarbon Prospectivity in Fold and Thrust Belts: A Global Review," in *Deformation of the Continental Crust: The Legacy of Mike Coward*, eds. A. C. Ries, R. W. H. Butler, and R. H. Graham (Geological Society of London Special Publications, 2007), 447–472.

37. D. Roeder, "Fold-Thrust Belts at Peak Oil," in *Hydrocarbons in Contractiona*, eds. G. P. Goffey, J. Craig, T. Needham, et al. (Geological Society of London Special Publications, 2010), 7–31.

38. EDGAR. *Emissions Database for Global Atmospheric Research (EDGAR)* (EDGAR, 2022).

39. RockWare. *PetraSim User Manual* (RockWare, 2022).

40. Y. Jung, G. S. H. Pau, S. Finsterle, and R. M. Pollyea, "TOUGH3: A New Efficient Version of the TOUGH Suite of Multiphase Flow and Transport Simulators," *Computers & Geosciences* 108 (2017): 2–7.

41. L. Pan, N. Spycher, C. Doughty, and K. Pruess, "ECO2N V2. 0: A TOUGH2 Fluid Property Module for Modeling CO_2-H_2O–NACL Systems to Elevated Temperatures of up to 300°C," *Greenhouse Gases: Science and Technology* 7 (2017): 313–327.

42. K. Pruess and N. Spycher, "ECO2N V2. 0: A TOUGH2 Fluid Property Module for Modeling CO_2–H_2O–NACL Systems to Elevated Temperatures of up to 300°C," *Energy Conversion and Management* 48 (2007): 1761–1767.

43. D. V. Nally, "A Stratigraphic and Sedimentologic Analysis of a Lower Atoka Sandstone, Frontal Ouachita Thrustbelt," in *AAPG Mid-Continent Section Meeting* (AAPG, 1995), 74–83.

44. Z. Al-Shaieb and P. Deyhim, "Chamosite, A Key Mineral for Interpretation of the Depositional Environment of the Spiro Sandstone," in *Marine Clastics in the Southern Midcontinent, 1997 Symposium: OGS Circular 103*, ed. K. S. Johnson (Oklahoma Geological Survey, 1997), 157–170.

45. J. M. Forgotson, H. Liu, H. Blatt, N. H. Suneson, and W. P. Schreiner, "Influence of Initial Calcite Grains and Diagenesis on Porosity Development in Spiro Sandstone of South Haleyville, South Hartshorne, and South Panola Fields, Pittsburg and Latimer Counties, Oklahoma," in *Marine Clastics in the Southern Midcontinent, 1997 Symposium: OGS Circular 103*, ed. K. S. Johnson (Oklahoma Geological Survey, 1997), 141–155.

46. J. S. Gross, S. A. Thompson, B. L. Claxton, and M. B. Carr, "Reservoir Distribution and Exploration Potential of the Spiro Sandstone in the Choctaw Trend, Arkoma Basin, Oklahoma and Arkansas," *AAPG Bulletin* 79, no. 2 (1995): 159–185, https://doi.org/10.1306/8D2B14E4-171E-11D7-8645000102C1865D.

47. C. R. D'Arlach, "Devonian Naturally Fractured Reservoirs, Tarija Basin, South America," AAPG International Conference and Exhibiton (AAPG, 2016).

48. M. T. van Genuchten, "A Closed-Form Equation for Predicting the Hydraulic Conductivity of Unsaturated Soils," *Soil Science Society of America Journal* 44, no. 5 (1980): 892–898.

49. D. Blackwell and M. Richards, "*Geothermal Map of North America*," AAPG Map (2004).

50. D. Blackwell, M. Richards, Z. Frone, et al., "Temperature at Depth Maps for the Conterminous US and Geothermal Resource Estimates," *GRC Transactions* 35 (2011): 1545–1550.

51. R. Mertens and J. Garcia, "One of the Deepest Wells Drilled in Bolivia: High Pressure and Temperature in More Than 9 Months of Drillings, no Casing Wear Detected," paper presented at the SPE Latin American and Caribbean Petroleum Engineering Conference, Virtual, July 2020..

52. A. S. Monasterio, V. Soriano, R. Cadena, R. Maldonado, and R. Ahmed, "First Successful Application of Wellbore Stabilization Technology Eliminates the Need for Contingency Casing and Differential Sticking Risk While Drilling Through Carboniferous-Devonian Formations: A Case Study on an Exploratory Well in the Sub Andean Bolivian Basin," paper presented at the SPE Latin American and Caribbean Petroleum Engineering Conference, Port of Spain, Trinidad and Tobago, June 2023.

53. F. P. Vieira and V. M. Hamza, "Assessment of Geothermal Resources of South America—A New Look," *International Journal of Terrestrial Heat Flow and Applications* 2 (2019): 46–57, https://doi.org/10.31214/ijthfa.v2i1.32.

54. A. A. Drake, A. K. Sinha, J. Laird, et al., "The Taconic Orogen," in *The Geology of North America Volume F-2*, ed. R. D. Hatcher, W. A. Thomas, and G. W. Viele (The Geological Society of America, 1989), 101–178.

55. P. H. Osberg, J. F. Tull, P. Robinson, R. Hon, and J. Robert Butler, "The Acadian Orogen," in *The Geology of North America Volume F-2*, ed. R. D. Hatcher, W. A. Thomas, and G. W. Viele (The Geological Society of America, 1989), 179–222.

56. R. D. Hatcher, W. A. Thomas, P. A. Geiser, et al., "The Alleghanian Orogen," in *The Geology of North America Volume F-2*, ed. R. D. Hatcher, W. A. Thomas, and G. W. Viele (The Geological Society of America, 1989), 233–318.

21523878, 0, Downloaded from https://scijournals.onlinelibrary.wiley.com/doi/10.1002/ghg.2365 by Virginia Polytechnic Institute, Wiley Online Library on [14/08/2025]. See the Terms and Conditions (https://onlinelibrary.wiley.com/terms-and-conditions) on Wiley Online Library for rules of use; OA articles are governed by the applicable Creative Commons License

57. S. J. Tewalt and L. F. Ruppert, “Coal Assessments and Coal Research in the Appalachian Basin,” in *Coal and Petroleum Resources in the Appalachian Basin: Distribution, Geologic Framework, and Geochemical Character*, ed. L. Ruppert and R. Ryder (USGS, 2014), 19.

58. M. J. Bartholomew, “Structural Evolution of the Pulaski Thrust System, Southwestern Virginia,” *GSA Bulletin* 99, no. 4 (1987): 491–510, https://doi.org/10.1130/0016-7606(1987)99⟨491:SEOTPT⟩2.0.CO;2.

59. H. J. Bauerlein, “Geology of the Millers Cove area, Roanoke, Craig and Montgomery Counties, Virginia” (M.S. Thesis, Virginia Polytechnic Institute, 1966).

60. P. L. Broughton, “Structural Geology of the Pulaski-Salem Thrust Sheet and the Eastern End of the Christiansburg Window, Southwestern Virginia” (M.S. Thesis, Virginia Polytechnic Institute and State University, 1971).

61. L. Wickstrom, E. Venteris, J. Harper, et al. *Characterization of Geologic Sequestration Opportunities, MRCSP Region Midwest Regional Carbon Sequestration Partnership Phase I Report, United States Department of Energy* (2005): 145 p.

62. L. W. Koehn, P. S. Prince, W. Godbey, et al., “First-Order CO_2 Trapping Characteristics of Fold-and-Thrust Belts: Assessing Carbon Storage Potential in the Appalachian Basin and Beyond,” *Leading Edge* 42 (2023): 726–799, https://doi.org/10.1190/tle42110755.1.

63. Virginia Energy, Geophysical Logs Database Well API#: 450230000100 (Columbia Natural Resources LLC, 1981), https://www.energy.virginia.gov/dgoinquiry/frmMain.aspx?ctl=10.

64. G. N. Breit. United States Geological Survey Produced Waters Database (2002), https://www.usgs.gov/tools/us-geological-survey-national-produced-waters-geochemical-database-ver-30-december-2023.

65. M. A. Engle and E. L. Rowan, “Geochemical Evolution of Produced Waters From Hydraulic Fracturing of the Marcellus Shale, Northern Appalachian Basin: A Multivariate Compositional Data Analysis Approach,” *International Journal of Coal Geology* 126 (2014): 45–56, https://doi.org/10.1016/j.coal.2013.11.010.

66. G. Rosen, A. Raddatz, T. Rodosta, et al., “Carbon Storage Assurance Facility Enterprise (CarbonSAFE): Carbon Storage Infrastructure Development for a Sustainable Future,” in Proceedings of the 17th Greenhouse Gas Control Technologies Conference (GHGT-17) 20–24 October 2024 (IEAGHG, 2024), https://doi.org/10.2139/ssrn.5069174.

67. G. W. Viele, “The Ouachita Orogenic Belt,” in *The Geology of North America Volume F-2*, ed. R. D. Hatcher, W. A. Thomas, and G. W. Viele (The Geological Society of America, 1989), 555–562.

68. A. E. Blythe, A. Sugar, and S. P. Phipps, “Structural Profiles of Ouachita Mountains, Western Arkansas,” *AAPG Bulletin* 72, no. 7 (1988): 810–819.

69. J. A. Curiale, “Petroleum Occurrences and Source-Rock Potential of the Ouachita Mountains, Southeastern Oklahoma,” *Oklahoma Geological Survey Bulletin* 135 (1983): 1–72.

70. P. A. Chenoweth, “Hydrocarbons of the Ouachita Trend,” in *The Geology of North America Volume F-2*, ed. R. D. Hatcher, W. A. Thomas, and G. W. Viele (The Geological Society of America, 1989), 739–746.

71. L. D. Meckel, D. G. Smith, and L. A. Wells, “Ouachita Foredeep Basins: Regional Paleogeography and Habitat of Hydrocarbons,” in *Foreland Basins and Fold Belts*, ed. R. W. Macqueen and D. A. Leckie (AAPG, 1992), 427–444.

72. K. S. Johnson, R. A. Northcutt, and G. C. Hinshaw, “Petroleum Production From Marine Clastics in Oklahoma,” in *Marine Clastics in the Southern Midcontinent, 1997 Symposium: OGS Circular 103*, K. S. Johnson (Oklahoma Geological Survey, 1997), 1–18.

73. M. R. Hepner, *Geometry of Late Paleozoic Thrusting, Wilburton and Damon Quadrangles, Arkoma Basin, Southeast Oklahoma* (Oklahoma State University, 2006).

74. S. Akhtar, *The Geometry of Thrust System in the Wilburton Gas Field and Surrounding Latimar County* (Oklahoma State University, 1995).

75. C. J. Banks and J. Warburton, “‘Passive-Roof’ Duplex Geometry in the Frontal Structures of the Kirthar and Sulaiman Mountain Belts, Pakistan,” *Journal of Structural Geology* 8, no. 3/4 (1986): 229–237, https://doi.org/10.1016/0191-8141(86)90045-3.

76. P. Baby, G. Hérail, R. Salinas, and T. Sempere, “Geometry and Kinematic Evolution of Passive Roof Duplexes Deduced From Cross Section Balancing: Example From the Foreland Thrust System of the Southern Bolivian Subandean Zone,” *Tectonics* 11, no. 3 (1992): 523–536, https://doi.org/10.1029/91TC03090.

77. T. A. McGilvery and D. W. Houseknecht, “Depositional Systems and Diagenesis of Slope and Basin Facies, Atoka Formation, Arkoma Basin,” in Marine Clastics in the Southern Midcontinent, 1997 Symposium: OGS Circular 103, ed. K. S. Johnson (Oklahoma Geological Survey, 1997), 129–140.

78. J. T. Birkholzer, A. Cihan, and Q. Zhou, “Impact-Driven Pressure Management via Targeted Brine Extraction—Conceptual Studies of CO2 Storage in Saline Formations,” *International Journal of Greenhouse Gas Control* 7 (2012): 168–180.

79. T. A. Buscheck, J. M. Bielicki, J. A. White, et al., “Pre-Injection Brine Production in CO_2 Storage Reservoirs: An Approach to Augment the Development, Operation, and Performance of CCS While Generating Water,” *International Journal of Greenhouse Gas Control* 54 (2016): 499–512.

80. B. K. Horton, “Tectonic Regimes of the Central and Southern Andes: Responses to Variations in Plate Coupling During Subduction,” *Tectonics* 37, no. 2 (2018): 401–679.

81. B. K. Horton and P. G. DeCelles, “The Modern Foreland Basin System Adjacent to the Central Andes,” *Geology* 25, no. 10 (1997): 895–898, https://doi.org10.1130/0091-7613(1997)025⟨0895:TMFBSA⟩2.3.CO;2.

82. I. Moretti, P. Baby, E. Mendez, and D. Zubieta, “Hydrocarbon Generation in Relation to Thrusting in the Sub Andean Zone From 18 to 22 Degrees S, Bolivia,” *Petroleum Geoscience* 2 (1996): 17–28, https://doi.org/10.1144/petgeo.2.1.17.

83. L.-B. Ouyang, “New Correlations for Predicting the Density and Viscosity of Supercritical Carbon Dioxide Under Conditions Expected in Carbon Capture and Sequestration Operations,” *Open Petroleum Engineering Journal* 4 (2011): 13–21.

84. B. Pan, X. Yin, and S. Iglauer, “Rock-Fluid Interfacial Tension at Subsurface Conditions: Implications for H_2, CO_2 and Natural Gas Geo-Storage,” *International Journal of Hydrogen Energy* 46, no. 50 (2021): 25578–25585, https://doi.org/10.1016/j.ijhydene.2021.05.067.

85. L. Koehn, B. Romans, and R. M. Pollyea, “Assessing Reservoir Performance for Geologic Carbon Sequestration in Offshore Saline Reservoirs,” *Energy Advances* 2 (2023): 2069–2084.

86. E. W. Conley, C. R. Chambers, J. B. Ogunleye, et al., “Pressure Management Strategies for Large-Scale Aquifer Recharge: Mitigating the Potential for Injection-Induced Earthquakes,” *Journal of Hydrology* 653 (2025): 132767, https://doi.org/10.1016/j.jhydrol.2025.132767.

87. M. Alghannam and R. Juanes, “Understanding Rate Effects in Injection-Induced Earthquakes,” *Nature Communications* 11 (2020): 3053, https://doi.org/10.1038/s41467-020-16860-y.

88. J.-P. Nicot and S. Hovorka, “Leakage Pathways From Potential CO_2 Storage Sites and Importance of Open Traps: Case of the Texas Gulf Coast,” in *Carbon Dioxide Sequestration in Geological Media—State of the Science. AAPG Studies in Geology*, ed. M. Grobe, J. C. Pashin, and R. L. Dodge (AAPG, 2009), 321–334.

89. A. P. Bump and S. D. Hovorka, “Fetch-Trap Pairs: Exploring Defintion of Carbon Storage Prospects to Increase Capacity and Flexibility in Areas With Competing Uses,” *International Journal of Greenhouse Gas Control* 122 (2023): 103817, https://doi.org/10.1016/j.ijggc.2022.103817.

21523878, 0, Downloaded from https://scijournals.onlinelibrary.wiley.com/doi/10.1002/ghg.2365 by Virginia Polytechnic Institute, Wiley Online Library on [14/08/2025]. See the Terms and Conditions (https://onlinelibrary.wiley.com/terms-and-conditions) on Wiley Online Library for rules of use; OA articles are governed by the applicable Creative Commons License

90. A. P. Bump and S. D. Hovorka, “Pressure Space: The Key Subsurface Commodity for CCS,” *International Journal of Greenhouse Gas Control* 136 (2024): 104174, https://doi.org/10.1016/j.ijggc.2024.104174.

91. F. Cappa, Y. Guglielmi, C. Nussbaum, L. D. Barros, and J. Birkholzer, “Fluid Migration in Low-Permeability Faults Driven by Decoupling of Fault Slip and Opening,” *Nature Geoscience* 15 (2022): 747–751.

92. W. L. Ellsworth, A. L. Llenos, A. F. McGarr, et al., “Increasing Seismicity in the US Mid-Continent: Implications for Earthquake Hazard,” *Leading Edge* 34, no. 6 (2015): 602–728, https://doi.org/10.1190/tle34060618.1.

93. W. L. Ellsworth, “Injection-Induced Earthquakes,” *Science* 341, no. 6142 (2013): 1225942, https://doi.org/10.1126/science.1225942.

94. M. Weingarten, S. Ge, J. W. Godt, B. A. Bekins, and J. L. Rubinstein, “High-Rate Injection Is Associated With the Increase in U.S. Mid-Continent Seismicity,” *Science* 348, no. 6241 (2015): 1336–13340, https://doi.org/10.1126/science.aab1345.

95. R. M. Pollyea, M. C. Chapman, R. S. Jayne, and H. Wu, “High Density Oilfield Wastewater Disposal Causes Deeper, Stronger, and More Persistent Earthquakes,” *Nature Communications* 10 (2019): 3077, https://doi.org/10.1038/s41467-019-11029-8.

96. NRC. *Induced Seismicity Potential in Energy Technologies* (The National Academies Press, 2013).

97. S. Ge and S. MO, “Induced Seismicity During Geoenergy Development—A Hydromechanical Perspective,” *Journal of Geophysical Research: Solid Earth* 127, no. 3 (2022): 1–34, https://doi.org/10.1029/2021JB023141.

98. M. O. Saar and M. Manga, “Seismicity Induced by Seasonal Groundwater Recharge at Mt. Hood,” *Oregon Earth and Planetary Science Letters* 214, no. 3–4 (2003): 605–618, https://doi.org/10.1016/S0012-821X(03)00418-7.

99. M. D. Zoback and S. Hickman, “In Situ Study of the Physical Mechanisms Controlling Induced Seismicity at Monticello Reservoir, South Carolina,” *Journal of Geophysical Research: Solid Earth* 87, no. B8 (1982): 6959–6974.

100. R. M. Pollyea, M. C. Chapman, C. R. Chambers, et al., “Introducing the Hampton Roads Seismic Network: Minimizing the Risk of Injection-Induced Seismicity in Virginia,” in OCEANS 2022 (IEEE, 2022), 1–8.

101. E. Conley, C. R. Chambers, J. Heisig-Mitchell, D. Holloway, and R. M. Pollyea, “Utilizing Numerical Simulation to Understand the Implications of Injection-Induced Seismicity for Managed Aquifer Recharge in Coastal Virginia,” in OCEANS 2022. (IEEE, 2022), 1–8.

102. D. R. Harp, P. H. Stauffer, D. O’Malley, et al., “Development of Robust Pressure Management Strategies for Geologic CO_2 Sequestration,” *International Journal of Greenhouse Gas Control* 64 (2017): 43–59.

103. J. A. White and W. Foxall, “Assessing Induced Seismicity Risk at CO_2 Storage Projects: Recent Progress and Remaining Challenges,” *International Journal of Greenhouse Gas Control* 49 (2016): 413–424, https://doi.org/10.1016/j.ijggc.2016.03.021.

104. M. D. Zoback and S. M. Gorelick, “Earthquake Triggering and Large-Scale Geologic Storage of Carbon Dioxide,” *Proceedings of the National Academy of Sciences of the United States of America* 109, no. 26 (2012): 10164–10168, https://doi.org/10.1073/pnas.1202473109.

105. M. D. Zoback and S. M. Gorelick, “To Prevent Earthquake Triggering, Pressure Changes Due to CO_2 Injection Need to be Limited,” *Proceedings of the National Academy of Sciences of the United States of America* 112, no. 33 (2015): E4510, https://doi.org/10.1073/pnas.1508533112.

106. N. Deichmann and D. Giardini, “Earthquakes Induced by the Stimulation of an Enhanced Geothermal System Below Basel (Switzerland),” *Seimological Research Letters* 80, no. 5 (2009): 784–798, https://doi.org/10.1785/gssrl.80.5.784.

107. A. L. Stork, J. P. Verdon, and J. M. Kendall, “The Microseismic Response at the In Salah Carbon Capture and Storage (CCS) Site,” *International Journal of Greenhouse Gas Control* 32 (2015): 159–171, https://doi.org/10.1016/j.ijggc.2014.11.014.

108. J. P. Verdon and A. Wüstefeld, “Measurement of the Normal/Tangential Fracture Compliance Ratio (ZN/ZT) During Hydraulic Fracture Stimulation Using S-Wave Splitting Data,” *Geophysical Prospecting* 61, no. S1 (2013): 461–475, https://doi.org/10.1111/j.1365-2478.2012.01132.x.

109. O. Ferrer, P. Santolaria, J. A. Muñoz, et al., “Analogue Modeling as a Tool to Assist Seismic Structural Interpretation in the Andean Fold-and-Thrust Belt,” in *Andean Structural*, ed. G. Zamora and A. Mora (Elsevier, 2022), 43–61.

110. R. D. Hatcher, A. L. Odom, T. Engelder, et al., “Characterization of Appalachian Faults,” *Geology* 16, no. 2 (1988): 178–181, https://doi.org/10.1130/0091-7613(1988)016⟨0178:COAF⟩2.3.CO;2.

111. M. R. Brudzinski and M. Kozłowska, “Seismicity Induced by Hydraulic Fracturing and Wastewater Disposal in the Appalachian Basin, USA: A Review,” *Acta Geophysica* 67 (2019): 351–364, https://doi.org/10.1007/s11600-019-00249-7.

112. W.-Y. Kim, “Induced Seismicity Associated With Fluid Injection Into a Deep Well in Youngstown, Ohio,” *Journal of Geophysical Research: Solid Earth* 118, no. 7 (2013): 3506–3518, https://doi.org/10.1002/jgrb.50247.

113. R. J. Skoumal, M. R. Brudzinski, B. S. Currie, and J. Levy, “Optimizing Multi-Station Earthquake Template Matching Through Re-Examination of the Youngstown, Ohio Sequence,” *Earth and Planetary Science Letters* 405 (2014): 274–280, https://doi.org/10.1016/j.epsl.2014.08.033.

114. S. G. Holtkamp, M. R. Brudzinski, and B. S. Currie, “Regional Detection and Monitoring of Injection-Induced Seismicity: Application to the 2010–2012 Youngstown, Ohio Seismic Sequence,” *AAPG Bulletin* 99, no. 9 (2015): 1671–1688, https://doi.org/10.1306/03311513194.

115. P. A. Friberg, G. M. Besana-Ostman, and I. Dricker, “Characterization of an Earthquake Sequence Triggered by Hydraulic Fracturing in Harrison County,” *Ohio Seimological Research Letters* 85, no. 6 (2014): 1295–1307, https://doi.org/10.1785/0220140127.

116. NETL, *Best Practices: Site Screening, Site Selection, and Site Characterization for Geologic Storage Projects DOE/NETL-2017/1844* (NETL, 2017).

117. M. R. Plampin, S. T. Anderson, S. Finsterle, et al., “Dynamic Estimates of Geologic CO2 Storage Resources in the Illinois Basin Constrained by Reinjectivity of Brine Extracted for Pressure Management,” *Greenhouse Gases: Science and Technology* 13, no. 1 (2023): 31–47, https://doi.org/10.1002/ghg.2189.

118. M. F. Coffin, L. M. Gahagan, L. A. Lawver, and L. W. D. Dalziel, Large Igneous Provinces: Map and Data, *Geophysics Technical Report No 221* (University of Texas Institute, 2013).

119. G. Goffrey, J. Craig, T. Needham, et al., “Fold-Thrust Belts: Overlooked Provinces of Justifiably Avoided?” in *Hydrocarbons in Contractiona* (Geological Society of London, 2010), 1–6.

120. L. Douglas, “Wolf Carbon Solutions Seeks End to Carbon Pipeline Application in Illinois,” *Reuters News* November 21, 2023.

121. J. Dura, “Navigator Cancels Proposed Midwestern CO2 Pipeline, Citing ‘Unpredictable’ Regulatory Process,” *Associated Press News* October 20, 2023.

122. J. Orledge, “Summit’s Carbon Storage Plans Face Strong Objections at ND Permit Hearing,” *Nebraska Examiner* June 16, 2024.

21523878, 0, Downloaded from https://scijournals.onlinelibrary.wiley.com/doi/10.1002/ghg.2365 by Virginia Polytechnic Institute, Wiley Online Library on [14/08/2025]. See the Terms and Conditions (https://onlinelibrary.wiley.com/terms-and-conditions) on Wiley Online Library for rules of use; OA articles are governed by the applicable Creative Commons License